Atomistic Modeling of Dislocations in Nanopillars

NTNU

Marit Olaisen

June 2015

THE NORWEGIAN UNIVERSITY
OF SCIENCE AND TECHNOLOGY
DEPARTMENT OF ENGINEERING DESIGN
AND MATERIALS

MASTER THESIS SPRING 2015
FOR
STUD.TECHN. MARIT OLAISEN

Atomistic Modeling of Dislocations in Nanopillars

Atomistisk modellering av dislokasjoner i nanopilarer

Modeling of the material properties at the nanoscale has become a reality. We have efficient and reliable programs, such as LAMMPS, and supercomputers, such as VILJE, available. In this Thesis the goal is to model the dislocation activity in pillars made of pure iron.

We experience that the strength of the pillars increases with reducing dimensions. This effect is explained on the basis of dislocation models, such as dislocation starvation and appearance of truncated dislocations. Programs are available to efficiently introduce dislocations in pillars, and hence to examine their effects on the mechanical properties.

The following tasks shall be performed

-Review the proposed theories and experimental results to explain the effect of pillar dimensions on the mechanical properties

-Present the common dislocation theories and mechanisms for pure iron, and how they depend on temperature and crystallographic orientations

-Perform atomistic modeling of pillars with introduction of dislocations. Parameters to be examined includes: number of dislocations, type of dislocation, slip orientations, temperature and specimen size

-The candidate can also perform own nanomechanical testing, including EBSD; FIB and loading with nanoindentation equipment.
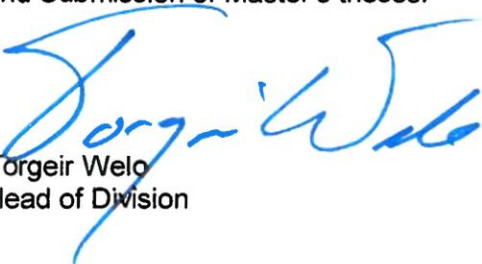
Formal requirements:

Three weeks after start of the thesis work, an A3 sheet illustrating the work is to be handed in. A template for this presentation is available on the IPM's web site under the menu "Masteroppgave" (http://www.ntnu.no/ipm/masteroppgave). This sheet should be updated one week before the master's thesis is submitted.

Risk assessment of experimental activities shall always be performed. Experimental work defined in the problem description shall be planed and risk assessed up-front and within 3

weeks after receiving the problem text. Any specific experimental activities which are not properly covered by the general risk assessment shall be particularly assessed before performing the experimental work. Risk assessments should be signed by the supervisor and copies shall be included in the appendix of the thesis.

The thesis should include the signed problem text, and be written as a research report with summary both in English and Norwegian, conclusion, literature references, table of contents, etc. During preparation of the text, the candidate should make efforts to create a well arranged and well written report. To ease the evaluation of the thesis, it is important to cross-reference text, tables and figures. For evaluation of the work a thorough discussion of results is appreciated.

The thesis shall be submitted electronically via DAIM, NTNU's system for Digital Archiving and Submission of Master's theses.

Torgeir Welo
Head of Division

Christian Thaulow
Professor/Supervisor

NTNU
Norges teknisk-
naturvitenskapelige universitet
Institutt for produktutvikling
og materialer

Preface

This master's thesis is written as a part of obtaining a Master's degree in material science and engineering at the Norwegian University of Science and Technology (NTNU). As a part of the program of study, the main profile 2; Materials Development and Properties, has been chosen as specialization. From there on it was chosen to write this master's thesis for the Department of Engineering Design and Materials (IPM), where the supervisor has been Professor Christian Thaulow. This thesis can be regarded as a continuation of the project work performed this autumn, which was titled *Atomistic modelling of deformation and fracture* [1]. Originally the duration of the work behind this thesis was set to 20 weeks, but due to technical problems with some of the equipment used, the deadline was extended by 5 days.

The main part of the work behind this thesis was the creation of computer simulations. In order to get a better overall understanding of the simulated situations, it was also chosen to include some experimental work. The experimental testing was closely related to the simulations in the way that they both were based on nanomechanical compression of nano-/microsized pillars of iron. However the main focus of the two parts of the thesis was different, as well as some of the conditions. The mandatory risk assessment of this master's thesis is included in the Appendix.

I have quite enjoyed working with this master's thesis as I have found the topic very interesting. I have gotten valuable help and input along the way, and feel that I have learned a lot in the process. First of all I would like to thank my supervisor Professor Christian Thaulow for giving me the opportunity to work with this thesis, and for always being supportive and enthusiastic about my project. Then I would like to thank PdD student Jørn Skogsrud and Postdoc Bjørn Rune Rogne for spending a lot of their time guiding me in my work, for helping me when I could not get my computer to stop yelling "error" and for always being welcome at their office. I would also like to thank PhD student Håkon A. H. Gundersen for frequently contributing to the conversations and explaining basic geometry when our brains failed us, and Inga G. Ringdalen at SINTEF for showing interest for my project and continually contributing with expertise, tips and suggestions regarding the dislocations. Finally I would like to thank PhD student Anette B. Hagen whom I have been working together with on the experimental part of the thesis.

Abstract

In this master's thesis, atomistic simulations of displacement controlled compression were performed on nanopillars consisting of pure iron. The main part of the work has been put into developing compression simulations of nanopillars with initial dislocations. The purpose of these simulations has mainly been to see if the addition of dislocations prior to deformation of the material, would visibly affect the material properties. Three models of the pillar were developed with different number and positions of dislocations. The simulations were performed both at room temperature and at 15K in order to see how the different temperatures would affect the dislocation behaviour and the overall results. During the work with the thesis, it was also decided to include simulations with different strain rates. All the simulations in this thesis were performed with the simulation tool/code LAMMPS (Large-scale Atomic/Molecular Massively Parallel Simulator) [2] with help from NTNU's supercomputer Vilje [3]. The dislocations were inserted using the program Atomsk [4], and the result was visualized in the analysis software Ovito [5].

In addition to performing atomistic simulations, a part regarding experimental compression testing of micro sized iron pillars were included. The goal of this part of the thesis was to get a better understanding of the experimental tests which the pillar simulations are based on. The experimental testing was performed in close collaboration with PhD student Anette B. Hagen.

The results showed that the insertion of dislocations into the simulated pillar did not visibly affect the mechanical properties of the sample. Neither the number nor position of dislocations seemed to have any influence on the stress-strain curves acquired from the simulations. The strain rate however was discovered to have the most influence on the stresses measured during the simulations, both with regard to the magnitude and the quality of the results. The dislocation mechanisms observed corresponded well with existing literature as the dislocations showed different behaviour at different temperatures and different strain rates.

Sammendrag

I denne masteroppgaven ble atomistiske simuleringer av displacement kontrollerte kompresjoner utført på nanopilarer bestående av rent jern. Hoveddelen av arbeidet har vært fokusert på å utvikle kompresjonssimuleringer av nanopilarer med innlagte dislokasjoner. Målet med disse simuleringene har hovedsaklig vært å finne ut om tilføringen av dislokasjoner før deformering av materialet ville påvirke materialets egenskaper i en større grad. Tre modeller av pilaren ble utviklet med forskjellige antall og posisjoner av dislokasjoner. Simuleringene ble utført både ved romtemperatur og ved 15K for å se hvordan endringer i temperaturen ville påvirke dislokasjonenes oppførsel og det endelige resultatet. Under arbeidet med oppgaven ble det også bestemt å inkludere simuleringer med forskjellige tøyningshastigheter. Alle simuleringer i denne oppgaven ble utført med simuleringsverktøyet LAMMPS (Large-scale Atomic/Molecular Massively Parallel Simulator)[2] ved hjelp av NTNUs supercomputer Vilje [3]. Dislokasjonene ble lagt inn i pilarene med programmet Atomsk [4], og resultatene ble visualisert med programmet Ovito [5].

I tillegg til å utføre atomistiske simuleringer ble eksperimentell testing av jernpilarer i mikrostørrelse inkludert som en liten del av rapporten. Målet med denne delen var å få en bedre forståelse av de eksperimentelle testene som pilarsimuleringene er basert på. Den eksperimentelle delen av rapporten ble utført i samarbeid med PhD student Anette B. Hagen.

Resultatene i denne rapporten viser at egenskapene til pilaren ikke ble stort påvirket av tilføringen av dislokasjoner før kompresjon. Hverken antall dislokasjoner eller deres posisjon i pilaren hadde noen innvirkning på spennings-tøyningskurvene som ble konstruert fra simuleringsresultatene. Tøyningshastigheten ble derimot oppdaget å ha størst påvirkning på spenningene som ble målt under simuleringene, både med tanke på stressnivået og kvaliteten på spennings-tøyningskurvene. Dislokasjonsmekanismene som ble observert samsvarte godt med allerede eksisterende dokumentasjon, og dislokasjonene viste ulik oppførsel for ulike temperaturer og tøyningshastigheter.

Contents

III Results   41

1 | Introduction

As new technologies have become available in the later years, the interest for studying material properties at the nanoscale level has increased for researchers all over the world. It has been discovered that the mechanical properties of materials undergo drastic changes, and the material strength increases drastically, as the specimen size is decreased into the micro- and nanometer range. Experimental techniques and computer simulation methods has been developed in order to measure and understand the reason behind these new properties. One of these techniques is the compression/indentation of micropillars, machined by the use of a FIB (Focused Ion Beam).

The Norwegian oil industry have in the later years developed an increasing interest in development of new material and alloys capable of withstanding the harsh climate in arctic regions, as it is believed that a high amount of undiscovered resources are located in these regions in the north. The mechanical properties of the materials currently used in the industry is not sufficient to handle the low temperatures and amount of stress the material will experience, as well as the desire for the materials to be lightweight, easy to transport and cost-effective. Therefore the industry has shown interest in the development of new materials based on the study of nanomechanics via Sintef's project on "Arctic materials" [6]. Steel is traditionally one of the most used materials in the world as it is relatively cheap and its alloys can have multiple uses. Some alloys of high quality steel can withstand some of the arctic conditions, but has been proven unsuitable for welding as the risk for brittle fracture is high [6]. Therefore research into the effect of temperature on the nanomechanical properties of steel is desired. The focus of this thesis though has been on the properties of pure iron, as a precursor and supplement to the current and future research on steel alloys.

Molecular Dynamic (MD) computer simulations have in this thesis been used as a supplement to ongoing experimental testing. The Atomistic Modelling and simulations in this thesis were created by the use of the code LAMMPS [2] which is based on classical molecular dynamics. By the use of computer simulations it is possible to study and observe detailed deformation mechanisms happening inside the material with much higher detail than what is possible through experimental testing, as the movements of individual atoms can be tracked. Though in order to get good simulation results, caution should be taken to make them as realistic as possible by for instance choosing an appropriate interatomic potential. For this thesis, initial dislocations have been inserted into the computer generated nanopillars in order to investigate and better understand the influence of these defects on the materials, and to see if they could possibly be some of the explanation behind dissimilarities in the stress-strain curves acquired previously from experiments and simulations. The theory behind Atomistic Modelling and Molecular Dynamics has previously been covered in the project work leading up to this master's thesis [1] and will therefore not be repeated here. For further information it is recommended to visit

the LAMMPS homepage [2] and the book *Atomistic Modelling of Materials Failure* by Markus Buehler [7].

Project assignment - Autumn 2014

As an introduction to working with a master's thesis, a project work with a similar topic was carried out [1]. This project dealt with atomistic simulations of iron nanopillars at two different sizes (diameter of 200Å and 290Å), three different orientations (compression in the [001]-, [149]- and [235]- directions) and with and without an initial dislocation. The goal was to insert a dislocation into the system to see whether or not the dislocation would affect the simulation results.

A few issues and possible sources of error was discussed. One of them was the size limitations of the program Atomsk, limiting the diameter size of the pillars to a maximum of 290Å. This limitation was overcome when working with the master's thesis, allowing for creation of dislocations in larger pillars (as will be seen later in the report). Another possible source of error was that the pillars became visible askew as dislocations were inserted. The reason behind this was believed to be the small size of the pillar, making the geometry sensitive to lattice changes caused by the insertion of the dislocation. The slight change in geometry might have affected the simulation results.

It was observed that the stress strain curves for the pillars with an initial dislocation had less fluctuations than the curves with a perfect lattice. It was also observed that for all the simulations, the dislocation quickly travelled to the surface of the pillar and disappeared without creating new dislocations. Sometimes the dislocation had left the system during the relaxation prior to the compression simulation itself. It was concluded in the report that displacement controlled loading of a pillar with a single dislocation would most likely not result in dislocation multiplication as the dislocation would leave the pillars before sufficient stress would be reached, supporting the dislocation starvation theory.

Part I

Theory

2 | Material deformation

In both the simulations and the experimental testing included in this thesis, the test specimen experience plastic deformation. Investigation of the different mechanisms behind these deformations are an important part of the thesis, and some theoretical background is therefore reviewed. Some of this theory was also included in the project work [1]. *Mechanical Metallurgy* by G.E. Dieter [8] and *Introduction to Dislocations* by D. Hull and D. J. Bacon [9] is recommended for further reading into the topics of both this and the next chapter.

2.1 Deformation of a crystalline structure

In solid metals, the atoms are normally arranged in three dimensional repeating patterns called a crystal structure as illustrated in Figure 2.1. Different materials prefer different kinds of crystal structures depending on the conditions under which it exists. In this thesis, both the simulations and the experimental testing were performed on pure iron which under normal circumstances has a BCC stucture.
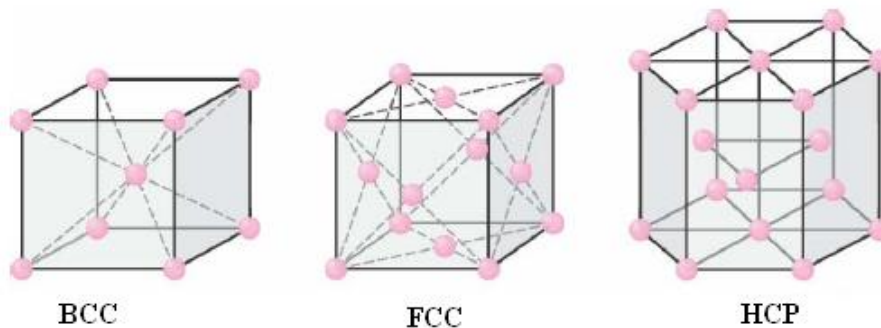

Figure 2.1: The three most common crystal structures; BCC, FCC and HCP [10]. BCC is the structure of the iron sample in both the simulations and the experimental testing in this thesis.

When a crystalline material is exposed to external pressure, it will at a certain limit start to deform plastically. When deforming a crystalline material, the directions in which the atoms are arranged closest together, the close packed directions, will be of interest. One of the most common ways of plastic deformation at elevated stresses, causing material failure, is slip. Slip can be seen as sliding a whole plane of atoms along another crystallographic plane of atoms. The planes for which a crystal is able to slip is denoted slip planes and are positioned along these close packed directions. For a BCC crystal lattice the highest density of atoms are along the <111>-directions, and the slip planes corresponding to these directions are the 110, 112 and 123 group of planes. Together these form the 48 slip systems of the BCC crystal lattice, Table 2.1.

Table 2.1: The 48 slip systems of a BCC crystal structure.

Crystal structure	Family of slip systems	Number of slip planes	Number of slip directions per plane	Number of slip systems
bcc	$\{110\}\ \langle111\rangle$	6	2	12
	$\{112\}\ \langle111\rangle$	12	1	12
	$\{123\}\ \langle111\rangle$	24	1	24

Theoretical strength of a material

The calculation of the theoretical strength of a material - the stress required to induce plastic deformation in a perfect crystal with no initial defects - was performed by Frenkel in 1926 [11]. The calculation was based on a the model in Figure 2.2 where deformation is caused by whole atomic planes sliding over each other by a co-operative movement of all the atoms in the plane. The shear stress required to move such a row of atoms away from their preferred place in a defined crystal structure and along another row of atoms was found out to theoretically be given by equation 2.1.

$$\tau = \frac{Gb}{2\pi a} sin \frac{2\pi x}{b} \tag{2.1}$$

Here G is the shear modulus of the material, b is the spacing between atoms in the direction of movement/direction of stress, a is the spacing between the rows of atoms and x is the shear translation of the two rows away from the low energy position of stable equilibrium. τ is the applied shear stress.
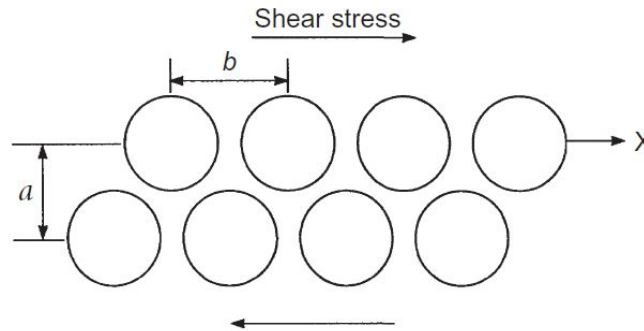

Figure 2.2: The shear stress applied to the structure is causing the two layers of atoms to slide over each other by a co-operative movement of all the atoms in each plane [9]

.

2.2 Slip mechanisms

As shown in table 2.1, slip always happens in the <111> directions for a BCC structure, but it can happen along three different slip planes. When a crystalline structure is exposed to external stress causing slip, which slip systems that activates can be highly dependent on the direction of the force applied. Therefore the yield stress of a material, the stress for which the material deforms plastically, is highly dependant on the material's crystal orientation. The critical resolved shear stress (CRSS) is the shear stress for which a slip system activates and results in slip [8], [9]. The orientation dependent relation between the critical resolved stress, and the magnitude and direction of the applied stress, is given by the Equation 2.2.

$$\tau_R = \frac{F cos\lambda}{A/cos\phi} = \frac{F}{A} cos\phi cos\lambda \tag{2.2}$$

$$m = cos\phi cos\lambda \tag{2.3}$$

This equation is denoted Scmid's law, and was developed by Schmid et al in 1935 [12]. The parameters used are illustrated in Figure 2.3 where F is the force affecting the system, A is the cross section of the cylinder, ϕ is the angle between the normal of the slip plane and the tensile axis, and λ is the angle between the slip plane/direction of slip and the tensile axis. The critical resolved shear stress, τ_R is along the direction of slip. The Equation 2.3 is denoted the Schmids factor and shows only the geometrical relation between the possible slip planes, where the slip system tending to activate is the one with the highest Schmid's factor. It can be seen from Figure 2.3 and Equation 2.3 that τ_R is at a maximum when $\phi = \lambda = 45°$.
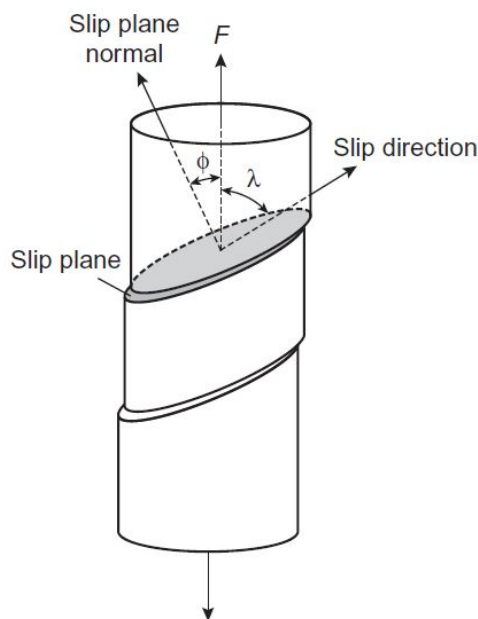

Figure 2.3: The stresses required to active a slip is dependent on the orientation of the slip plane in relation to the direction of force [9].

When $\phi = 90°$ og $\lambda = 90°$, there is no shear stress on the slip plane, and slip will therefore not occur. These equations are valid within a single crystal/within a grain where the crystal orientation is the same for the whole section. It has however been discovered that materials with a BCC structure does not always follow the Schmid's law, and it does happen that slip systems with a smaller Schmid's factor has been preferred over slip systems with a higher Schmid's factor.

2.3 Stress and strain

In this thesis, stress-strain curves are frequently used to describe the results from both the simulations and the experimental testing. The definitions of the nominal stress σ and strain ϵ calculated in this thesis are given by the Equations 2.4 and 2.5. Here, L_0 is the initial height of the pillar, P is the applied load and A_0 is the initial cross section of the pillar.

$$\varepsilon = \frac{\Delta L_0}{L_0} = \frac{L - L_0}{L_0} \tag{2.4}$$

$$\sigma = \frac{P}{A_0} \tag{2.5}$$

For the simulations, information about the average indenter force and the height of the pillar can be found in the simulation log. The average indenter force is given in the unit eV/Å which is the same as $1.6021773 \cdot 10^{-9}$N.

2.4 Size dependency

As the size of a test specimen is decreased into the micro and nano level, experiments have shown that the material undergoes a drastic change in yield stress. As the sample size gets smaller, the yield stress increases rapidly. This size dependent strength follows a power law given by Equation 2.6 where σ is the flow stress, K is the power law coefficient, D is the surface diameter at the top of the pillar and n is the power law exponent [13].

$$\sigma = KD^{-n} \tag{2.6}$$

This increase in strength is caused by a fundamental change in the mechanisms that are controlling the strength of the material; that is, the dislocation mechanisms inside the material changes. The reason behind this change, and which mechanisms that are now dominant is widely discussed. Many theories have been proposed, and some of them are highly likely to be important contributing factors to the strengthening effect. The topic is still under research though as there still are a lot of uncertainties as to whether these are the only reasons behind this effect, or if other mechanisms could take place under different circumstances. A collection of yield points measured for iron with different sample sizes are illustrated in Figure 2.4. This illustration shows clearly that the size of the specimen does matter in calculating the material strength.
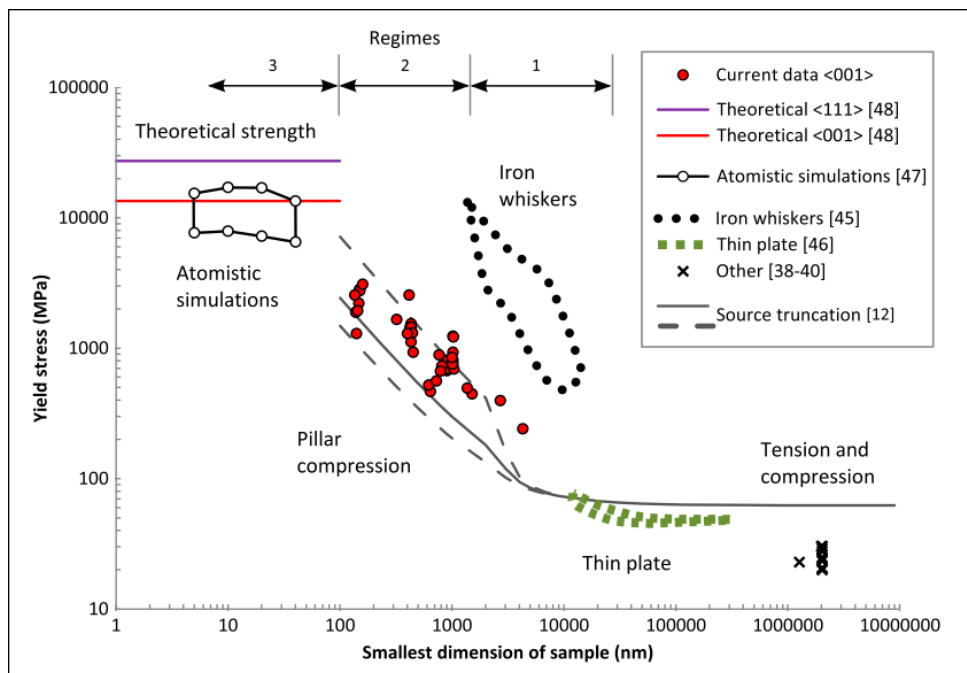

Figure 2.4: An overview of yield points reported for iron at various sample sizes. The data is gathered from multiple articles and papers [13].

In this thesis, the simulations have been performed on a pillar with diameter of 500Å, while the experimental testing have been performed on pillars with a diameter of approximately 1µm.

2.5 Strain rate

The strain rate is a measure of how much strain a specimen experiences per unit of time, as defined in Equation 2.7. As atomistic simulations are the result of an extensive amount of computer calculations, the time period over which it is possible to make such detailed simulations is very limited. Usually the unit for time in atomistic simulations is given in picoseconds, and the whole simulation therefore only cover a few hundred picoseconds. This results in strain rates which are several orders of magnitude larger than the strain rates expected from pillar compression testing, which normally could be of the magnitude 10^{-1} to $10^{-3} s^{-1}$ [13], [14]. The strain rates registered for the indentation tests carried out at NTNU are close to the latter.

$$\dot{\epsilon} = \frac{\epsilon}{t} \tag{2.7}$$

It is important to pay attention to these large differences in strain rate between simulations and experimental testing, as a change in strain rate could also lead to different mechanical properties of the material. It has for instance been discovered that by decreasing the strain rate of a simulation or an experiment, the measured yield strength decreases as well [14], [15]. It is also believed that the strain rate is likely to affect the measured stress values more at elevated temperatures.

A way of describing the strain rate dependency of measured stress by the use of Equation 2.8, was proposed in a conversation with one of NTNU's employees (2015, 30th April). Equation 2.8 was derived by combining data from Naamane et al [16] and Caillard [17] and has been suggested for describing the strain rate dependency of shear yield stress. Here, τ^* is the shear yield stress, $\tau^*(0K)$ is the shear stress at 0K, k is the Boltzmann constant which has the value $8.62 \cdot 10^{-5}$ eV/K, T is the temperature, $\dot{\epsilon}_\tau$ is the strain rate, and G_0^*, $\dot{\epsilon}_0$, q and p are material dependent constants. For BCC iron, the suggested values for the constants are $\tau^*(0K) = 365$MPa, $G_0^* = 0.84$eV, $\dot{\epsilon}_0 = 1 \cdot 10^8 s^{-1}$, $q = 1.43$ and $p = 0.7$.

$$\frac{\tau^*}{\tau^*(0K)} = \left[1 - \left\{ -\frac{kT}{G_0^*} ln(\frac{\dot{\epsilon}_\tau}{\dot{\epsilon}_0}) \right\}^{\frac{1}{q}} \right]^{\frac{1}{p}} \tag{2.8}$$

For atomistic simulations with a pillar diameter of 400Å, it has previously been experienced unreliable results at strain rates higher than 0.5-$1 \cdot 10^9 s^{-1}$ [15].

3 | Dislocation Theory

Since a perfect lattice in reality is nearly impossible to achieve, a material normally contains a lot of defects. There exist different kinds of defects, which include point defects (vacancies or interstitial atoms), line defects (dislocations), surface/planar defects (grain boundaries or stacking faults) or volume/bulk defects (voids or new phases) [9] . Defects can have a great inuence on the material properties and gaining a better understanding of them is therefore important. A main focus of the simulation part of this thesis will be on the line defects; dislocations.

3.1 Burgers vector

The Burgers vector plays an important role in defining dislocations and describing their behavior. In a crystal structure, the direction of the Burgers vector is along the line with the highest density of atoms. The iron simulated and tested in this thesis is, as previously mentioned, of BCC type crystal structure. For BCC, the direction of highest density of atoms is along the $<111>$ directions, and therefore this is also the direction of the Burgers vector. In a BCC crystal the slip planes corresponding to the $<111>$ directions are the $\{110\}$, $\{112\}$ and $\{123\}$ groups of planes. It might be worth noticing that the BCC structure does not have any true close packed planes, which will result in some of the slip systems being less inclined to activate at low temperatures [9].

$$| b | = \frac{a \cdot \sqrt{h^2 + k^2 + l^2}}{2} = \frac{a \cdot \sqrt{3}}{2} \tag{3.1}$$

The Burgers vector is closely connected to dislocations. In the next sections it can be seen that by making a burgers circuit around the dislocation in a crystal, Figures 3.1b and 3.2b, the Burgers vector is defined as the closure failure due to the dislocations present. The direction of the Burgers vector is also the direction of the dislocation movement. The magnitude of the Burgers vector is described by Equation 3.1, where a is the lattice length. For a BCC lattice h, k and l all will have the value 1.

3.2 Types of dislocations

Dislocations are line defects in a crystalline lattice. Dislocation creation and movement are often ways to release energy as a counter reaction to forces applied to the system, and results in the production of plastic deformation (dislocations are often a precursor to slip). A good way to visualize dislocations is to imagine planes in the crystal lattice sliding relative to each other to form a line in the structure for which the lattice is distorted. There are two main types of dislocations; edge and screw dislocations.

3.2.1 Edge dislocation

An edge dislocation can easiest be viewed as a lattice defect where an extra half-plane of atoms is inserted into the lattice, see Figure 3.1. The Burgers vector for an edge dislocation is always normal to the dislocation line. Because of this, an edge dislocation is positioned in a specific slip system.
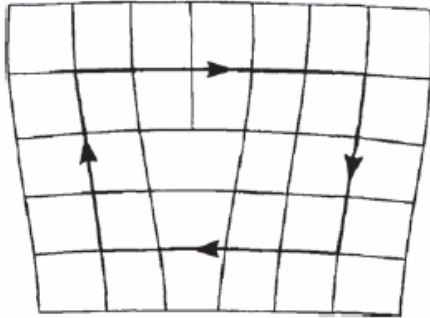
(a) Cross section of an edge dislocation in a crystal lattice with the Burgers circuit drawn.
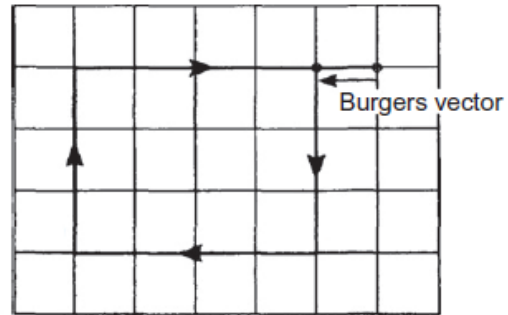
(b) The Burgers vector can be illustrated as the closure failure due to the dislocation present.

Figure 3.1: Illustration of an edge dislocation with the Burgers circuit drawn. By imagining restoring the lattice by removing the dislocation present, the Burgers vector appears from the Burgers circuit [9].

3.2.2 Screw dislocation

A screw dislocation can be seen as a defect caused by two planes sliding relative to each other and sort of twisting the lattice, see Figure 3.2. The Burgers vector for a screw dislocation is always parallel to the dislocation line. Because of this, a screw dislocation is not limited to a specific slip system.

(a) Illustration of a screw dislocation in a crystal lattice with the Burgers circuit drawn.
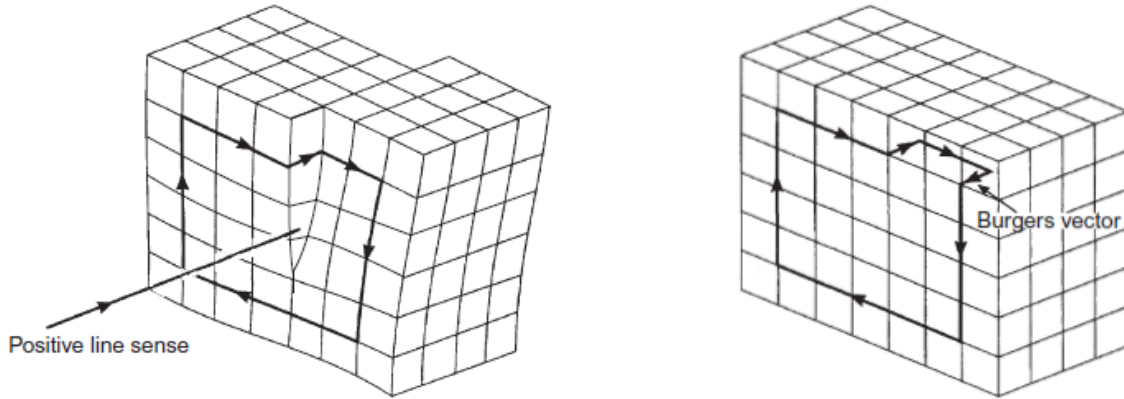
(b) The Burgers vector can be illustrated as the closure failure due to the dislocation present.

Figure 3.2: Illustration of a screw dislocation with the Burgers circuit drawn. By imagining restoring the lattice by removing the dislocation present, the Burgers vector appears from the Burgers circuit [9].

A dislocation can not end in the middle of a perfect lattice, so it always has to be connected to a surface or another material defect. In most real cases, a dislocation will be a mix between edge and screw dislocations. Therefore it does not necessary need to be a straight line, but can for instance form a loop with itself.

3.3 Dislocation glide and climb

When a material is under stress, the dislocations inside the material are often moving around, causing plastic deformation. There are two main ways for a dislocation to move; by glide or climb.

A dislocation is gliding when it moves along the surface defined by the slip system which contains both its dislocation line and Burgers vector. When many dislocations are moving in a specific slip plane, they can cause slip. For screw dislocations or screw segments in a mixed dislocation, cross slip can occur. This is when the dislocation chooses to switch/slip to another slip plane which contains the same Burgers vector. Dislocations move almost entirely by glide at low temperatures.

A dislocation is climbing if it moves outside of the slip plane it normally would glide in. That is, it moves in a direction normal to the burgers vector. Climbing usually requires thermal activation. Therefore, dislocation climb is most likely to happen at elevated temperatures.

3.3.1 Kink and Jog

When a dislocation moves by glide or climb, it often moves stepwise, bit for bit, and not the whole dislocation at once. When climbing, the steps created in the dislocation are called jogs. When moving in a glide plane, these steps are called kinks. Even though a screw dislocation does not have a specific glide plane it can move by creation of kinks. But by doing so, the kink parts of the dislocation will then be of edge character which *is* contained in a specific glide plane or will work as an anchor point for the rest of the screw dislocation. As kinks and jogs can act as anchor points for a dislocation, the dislocation sometimes choose to separate from the immobile parts, leaving them behind as a trail of debris.
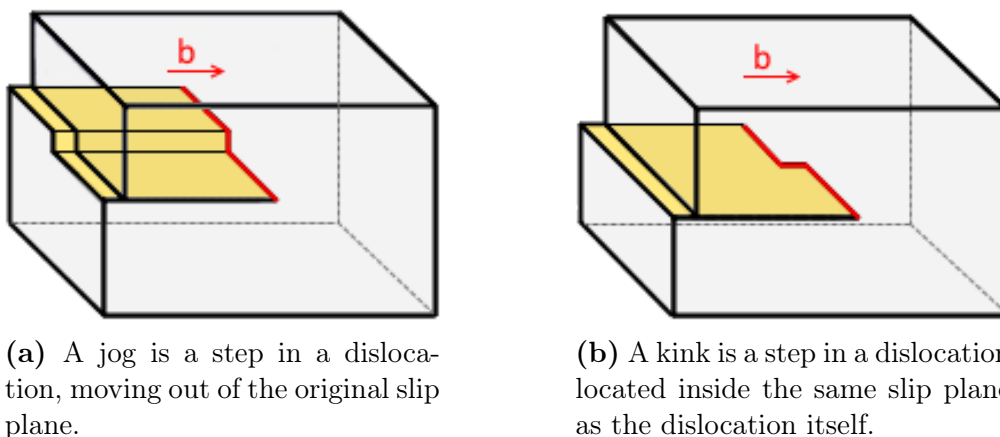

(a) A jog is a step in a dislocation, moving out of the original slip plane.

(b) A kink is a step in a dislocation located inside the same slip plane as the dislocation itself.

Figure 3.3: Illustration of jog and kink as they appear in an edge dislocation [18].

In a BCC structure, kink mechanisms are the main mechanism behind screw dislocation motion [19]. One of the most favorable ways to move by kink nucleation, is by the creation of double-kinks which then moves away from each other along the dislocation line - increasing the length of the newly created line between them. It has previously been

observed through simulations that at low temperatures the dislocations move smoothly by kink-pairs. At elevated temperatures cross-kink mechanisms can occur, causing the motion of the line to become uneven and leaving behind debris.

3.4 Dislocation starvation and multiplication

As previously mentioned, several theories have been proposed in order to try to explain the increase in strength as the material sample decreases in size. One of the main theories is that the strength is due to a dislocation starvation effect [20]. This theory states that as the pillar diameter decreases below a certain size, the theory of work hardening and multiplication of dislocations do no longer apply as any mobile dislocations existing in the sample would escape from the crystal at the nearest free surface. This would decrease the dislocation density of the pillar until it reaches a dislocation starved state, which requires high stresses in order to nucleate new dislocations. This theory corresponds well with the results from the simulations mentioned in the previous project assignment [1], where the dislocations inserted into the pillars escaped almost immediately.

Another proposed theory that was examined in the previous project was the dislocation multiplication theory, which stated that a BCC-structure was unlikely to be in a dislocation starved state as a dislocation will be able to multiply through dislocation loops as the pillar experiences high stress [21]. It was though concluded in the project report that during a displacement controlled simulation with gradually increasing stress, it was unlikely that a high enough stress would be reached in order to create dislocation multiplication before the dislocation would have had the opportunity to leave the pillar.

3.5 Dislocation density

Many previous simulations performed in order to measure the strength of nanopillars have assumed that the pillars are defect free, as it is easy to make a perfect crystallographic lattice when creating an atomistic model. This is however unlikely to be the case for a pillar that has been milled/fabricated, as the milling process itself is guarantied to inflict damage on the pillar surface which can lead to the creation of dislocations. TEM (Transmission Electron Microscopy) studies of molybdenum nanopillars fabricated by the use of FIB has been shown to have a dislocation density of approximately $10^{15}\mathrm{m}^{-2}$ [22]. This would correspond with an approximate total dislocation length of $2.5 \cdot 10^{3}$Å for the volume of a pillar with a diameter of 500Å and height of 2.5 times the diameter. It can therefore be assumed that a pillar of this size, theoretically fabricated by the use of FIB, would contain no more than five dislocations. Probably the number is closer to four, as the dislocations often are oriented with an angle to the surface and not along the pillar cross section.

4 | Experimental theory

4.1 EBSD (Electron Back Scatter Diffraction)

EBSD is a technique which is used to find the crystal orientation of a crystalline material sample. When performing an EBSD analysis, an electron beam is sent towards a tilted sample. The resulting backscatter electrons, having been diffracted by the atomic layers in the material will generate a characteristic diffraction pattern.

As different crystal structures and orientations will make different diffraction patterns, these patterns can be used to identify the crystallographic orientation of different grains in a crystalline material. This technique has prior to this project been used to create a map over the different orientations of the grains in the iron sample used for the pillar testing.
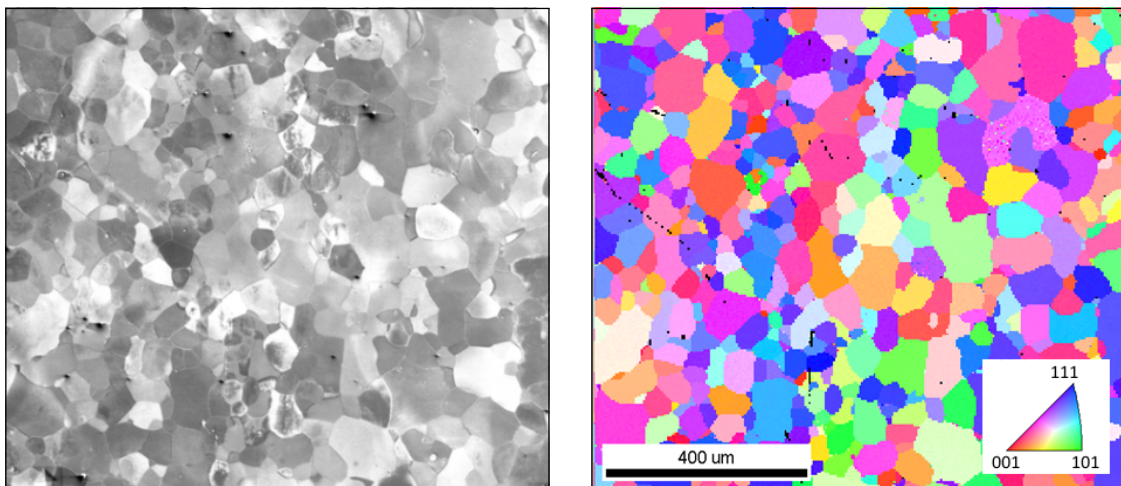
(a) A SEM picture of the sample surface

(b) An EBSD scan of the sample surface at the approximate same position as the SEM picture.

Figure 4.1: When performing an EBSD analysis, the grains at the sample surface is coloured according to the crystal orientation corresponding to the diffraction pattern registered from the different grains. The pictures are taken from the same position on the surface of the iron sample used in the experimental part of this thesis.

4.2 FIB (Focused Ion Beam)

The micro pillars used in the experimental testing part of this thesis are made by the use of FIB (Focused Ion Beam). In the FIB, a beam of high mass ions (usually Ga^+) are accelerated toward the sample surface. Due to the high mass and velocity of the ions, they damage the sample surface and sputter away some of the surface material. By controlling the current, the ion beam can be used to fabricate micro- and nanoscale structures on the sample surface.

When creating a structure by the use of FIB, the new surface created is slightly damaged due to the contact with the Ga^+ ions. It is also very likely that some of the Ga^+ ions have become embedded in the surface of the structure, creating unwanted defects. Very often, the FIB is combined with a SEM, a so-called DuamBeam FIB, in order to be able to take pictures of the surface and the structures created. By using an electron beam to generate pictures instead of an ion beam, less unwanted damage is done to the surface and the picture is of a much higher quality. The instrument used in this thesis is a DEI Helios NanoLab DualBeam FIB which is placed in a vibration isolated cleanroom at NTNU [23].

Figure 4.2: Picture of the FIB used in this project. The FIB is located at the NTNU Nanolab [23].

4.2.1 Tunneling effect

The amount of sample material sputtered away by the Ga^+ ions is dependent on the crystallographic orientation of the sample. As the Ga^+ ions collide with the surface, the crystallographic structure could be oriented in such a way that the spacing between the atoms gives the Ga^+ ions a clear path with few collisions on its way into the sample, in which case the sputtering yield is low. If the structure is oriented in such a way that the Ga^+ collides with a relatively large amounts of atoms, the sputtering yield is high. The milling parameters will therefore have to be changed in order to make the same structures in different crystallographic orientations. This is called the tunneling effect.

4.2.2 Redeposition

When material is sputtered away during the FIB milling process, some of the material might be redeposited to other areas on the sample surface. The redeposited material could alter the structures already created in the sample. This can especially be a problem when milling a crater in the surface as the sputtered atoms will redeposit the inside walls of the crater, counteracting the sputtering. Redeposition is the main reason why the fabricated micropillars have a tapering angle as the FIB is not able to remove all the material in a straight vertical line.

4.3 Indentation

Nanoindentation is originally a method used to measure the hardness and E modulus of a material. The nanoindenter is used to make an indent in the material surface while measuring the load required to do so. The hardness and E modulus can then be calculated from the resulting load-displacement curves acquired from loading and unloading the indenter. However, finding the hardness of the material is not the goal in this thesis. The indenter will instead be used to perform compression tests of FIB-milled micro pillars. The technique of using a nanoindenter device to perform compression of FIB-milled micropillars was developed by Uchic et al [24]. By using a flat indenter tip rather than a pointed one, one could continuously record load and displacement curves while compressing microsized pillars. By knowing the dimensions of the pillar compressed, one could convert the recorded load-displacement data to stress-strain curves as previously seen with Equations 2.5 and 2.4.

$$\sigma = \frac{P}{A_0} = \frac{4P}{\pi d_{top}^2} \tag{2.5}$$

Since this technique can be used to measure the stress required to deform pillars with a diameter less than 1 μm, the whole pillar to be tested could be milled inside a single grain and therefore consist of the same crystal orientation. The stress measured from deforming the pillar could therefore very likely be the stress required to activate a specific slip plane inside the particular orientation. What is also very useful is that due to the small pillar sizes, the activated slip planes can in many cases be observed in a SEM. The results acquired from these tests can depend a lot on the pillar geometry. Previously experiments and finite element modelling has shown that the ideal aspect ration of such a pillar (height/diameter) is between 2 and 3, and that the tapering angle is as small as possible. The tapering angle could be calculated from Equation 4.1 where α is the tapering angle, D_{base} is the diameter of the pillar base, D_{top} is the diameter of the pillar top and h is the pillar height.

$$\alpha = tan^{-1}(\frac{D_{base} - D_{top}}{2h}) \tag{4.1}$$

Part II

Experimental and Simulation procedure

5 | Simulation details/setup

When running computer simulations, it is first required to create a model of the system and define its initial conditions. While making the initial models for the simulations performed in this project work, it has been desirable to try to make them resemble the experimental test specimens as much as possible. Though there still has to be a compromise as computer and program limitations has to be taken into consideration as well. The interatomic potential chosen for the simulations in this project is the EAM potential developed by Mendelev et al. [25].

5.1 Pillar model and conditions

In this thesis, the pillar dimensions and a lot of the initial conditions were kept the same for the different pillars that were simulated. All the simulations were performed on pillars of BCC iron, and all the pillars were oriented so that the compressions were done in the [001]- direction. Though it would have been very interesting to examine the pillar and dislocation behavior at different crystallographic orientations, it was chosen not to do so in this thesis as examining other variables were prioritized. The influence of pillar orientation was briefly examined in the previous written report [1] leading up to this thesis, and would be a recommended variable for future simulations.

Table 5.1: The pillar size, pillar orientation and number of dislocations used in the simulation models.

Pillar diameter [Å]	Direction of compression	Temperature [K]
500	[001]	15, 300

As well as all the pillars being of BCC iron and having the same orientation, all the pillars were chosen to have a diameter of 500Å. This is much larger pillars than the ones simulated previously [1], as they were limited to a diameter of 290Å due to problems with inserting the dislocations. When the size of the pillars were so small, it was seen that they could easily be influenced by other factors than the mechanisms we wanted to observe, and could not as easily be comparable with the much larger test specimens. Ideally the pillar diameter should be much larger (at least 1000Å to be close to the same size as the experimental testing). Although this should theoretically be possible, it would require a lot more computer capacity. The simulations would be much more complex and require a long calculation time, a more powerful computer for visualization of the results and much more computer memory for the data acquired. Such large simulations are therefore at the moment not suited for a master's thesis. Taking this into consideration,

a diameter of 500Å is considered as a reasonable size for the simulations. The rest of the pillar dimensions as defined by the pillar diameter are illustrated in Figure 5.1. A 3° tapering angle of the pillar was also introduced to make it more realistic, as machining the experimental pillars never results in them being perfectly straight. The z-axis of the figure is the direction of compression, [001].
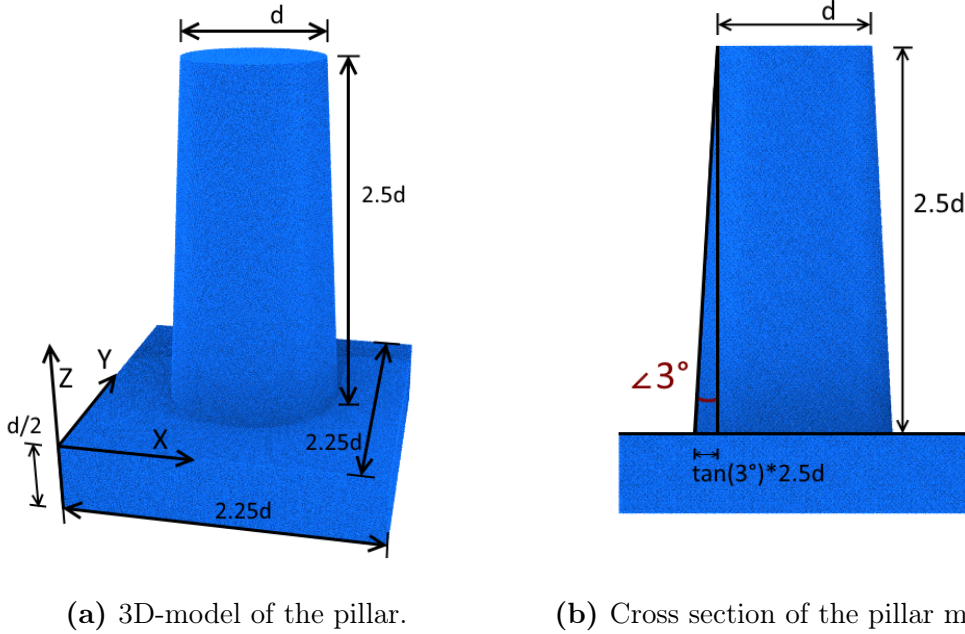

(a) 3D-model of the pillar.

(b) Cross section of the pillar model.

Figure 5.1: The illustrations show the pillar model which is used in all the simulations in this thesis. The dimensions of the pillar is included and defined by the pillar diameter d. The pillar model has a tapering angle of 3°.

In simulations, the borders of the system in the x-, y- and z-directions are defined by the simulations box. From the illustration of the pillar model, Figure 5.1, it can be seen that the system is designed so that the pillar is standing on a square base ending in the box borders in the x- and y-directions. But what is desired to simulate is the pillar standing on a bulk material. To simulate a pillar on a bulk material directly would be impossible as it would require a huge amount of atoms to make the base large enough. Since size is a limitation of simulations, the way to solve this problem is by making the system periodic at the box borders. The box will then repeat itself indefinitely in the directions specified and therefore act like a bulk material. In the simulations in this thesis that would be the x- and y-directions. When making the system periodic, the length of the sides of the box has to be adjusted so that they are a multiple of the lattice length to make sure that atoms are not overlapping at the borders, making the system unstable.

5.2 Simulation environment

Before starting the compression of the pillars, a relaxation of the system is run for a number of timesteps. For this relaxation, a NPT ensemble is chosen (constant pressure) [1]. This is because during the relaxation it is desired to have a constant pressure in order to let the atoms position themselves in equilibrium positions with no outside forces acting on them. During the main run however, constant pressure is not desired as the compression of the pillar would expand the system in order to compensate for the forces applied. Therefore, a NVT ensemble with constant volume is used after the relaxation is finished. The simulations in this project were set to do displacement controlled indentations of the pillar as this closest resembles the experimental testing performed on micropillars.

Table 5.2: The lattice length and Burgers vector for the different temperatures that were used in the simulations.

Temperature [K]	Lattice length [Å]	Length of Burgers vector [Å]
300	2.85896	2.4759
15	2.8552	2.4727

One of the variables that are examined in this thesis is the effect of different temperature on the system. Initially it was planned to run simulations at room temperature and -90°C as these are the temperatures most relevant to the experimental testing and the arctic materials program [6]. But in order to see changes and effects of the temperature more clearly it was recommended to simulate with a much lower temperature initially. Therefore, it was chosen to run simulations at the temperatures 300K and 15K. As the temperature of the system is changed, it is also important to note that the lattice length of the system will change accordingly, see table 5.2. It is therefore necessary to not only change the environment in which the simulation is run, but also to change the pillar model itself.

Table 5.3: The strain rate used in the simulations.

	Simulation run 1	Simulation run 2
Timestep [ps]	0.0015	0.0015
Number of timesteps (relaxation)	50 000	50 000
Number of timesteps (ramp)	-	20 000
Number of timesteps (main run)	300 000	900 000
Max strain	0.15	0.10
Length of main run [ps]	450	1350
Strain rate [/s]	$3.33 \cdot 10^8$	$0.74 \cdot 10^8$

The simulations in this thesis were mostly run at two different strain rates. At first,

simulations of model 1 and 2 and a "reference model" with no dislocations inserted were run at different temperatures and strain rate $3.33 \cdot 10^8 s^{-1}$. After reviewing the results from the first run of simulations, it was decided to do some changes to the script before running the simulation of model 3, and also to rerun the other simulations with some new parameters, see table 5.3. Due to the high strain rate in the first simulation run, the stress-strain curves showed high fluctuations. This made it difficult to see possible changes in the stress-strain curves for the different models as the high strain rate caused much more variation. The variations in the measured stress also made it difficult to get a clear impression of the curve itself, the E-modulus and yield point. The strain rate was therefore changed to $0.74 \cdot 10^8 s^{-1}$ for the second simulation run.

A new part was also included in the code between the relaxation and the main run. As the stress-strain curves from the first simulation run showed elevated stress when the compression started (when the indenter came in contact with the pillar), the velocity of the simulated indenter were changed from being constant throughout the whole simulation, to gradually increase from zero to the velocity corresponding with the chosen strain rate. Unfortunately it was discovered afterwards that the new part of the code had a small flaw, so that when the velocity reached the intended value, fixing the velocity caused the indenter to jump back a short distance, see Figure 5.2. This small jump however does not seem to have affected the results in a major way, and by "ramping" the velocity it seems that the pillar does not experience the same sudden increase in stress as the indentation starts. So for all intents and purposes the new part of the code did improve the simulation.
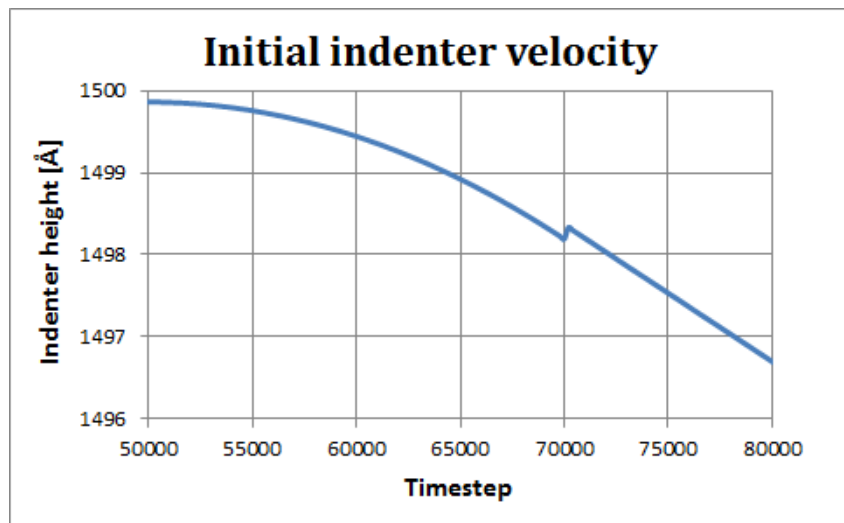

Figure 5.2: The velocity of the indenter, illustrated as change in indenter position per time step.

5.3 Insertion of dislocations in pillars

One of the main parts of this thesis is examining the effects of inserting initial dislocations into the pillars before the start of the simulations. To insert dislocations into the pillar model, the program/code Atomsk [4] developed by Pierre Hirel was used. This program was used and evaluated during the project work leading up to this thesis and it was concluded then that the results from using it for the most part were good and credible, and that it was the best alternative to efficiently insert dislocations into the pillar. As previously, the method used to insert dislocations is therefore to initially make the model in LAMMPS and import the file to Atomsk. In Atomsk the system is rotated and the dislocation can be inserted along one of the axis of the rotated system. The process is repeated for each additional dislocation one wants to add to the system, and finally the system is rotated back to its original position and the file is converted and imported back into LAMMPS. This works fairly well, though there still are a few issues occurring that will be discussed later.

In the beginning of the project it was considered to work both with screw and edge dislocations. Previously it has been chosen to only work with screw dislocations because screw dislocations move slower than an edge dislocation in a bcc structure. In previous testing the dislocations have had a strong tendency to leave the pillar very early in the simulations. Therefore this is still a valid reason to prioritize screw dislocations as they hopefully would stay in the pillar for a longer period of time. A few tests were done to try to insert edge dislocations into the pillar, but these were not successful as the crystal structure outside of the dislocation kept getting distorted. This was probably due to errors in the input command and not the program itself, but the process of locating the error was very time consuming. Considering both these facts, it was again decided to prioritize only to work with screw dislocations in this project and leave edge dislocations for later research.

Table 5.4: The initial dislocations inserted in the different models that were made.

System	Number of dislocations	Direction of Burgers vector
Model 1	2 { 1 1	[-111] [111]
Model 2	2 { 1 1	[-111] [111]
Model 3	5 { 2 2 1	[-111] [111] [-1-11]

In addition to a pillar without any initial dislocations, three different models of the pillar were made with different number and position of dislocations, see Table 5.4. These were all simulated at the two different temperatures and at two different strain rates. Though screw dislocations are not bound to a specific slip plane, a slip plane is defined in order to insert the dislocations and they can therefore initially be regarded as belonging

to a slip system. Previous testing showed that the screw dislocations had a tendency to want to move along the specified slip plane provided that the plane were close to 45° on the direction of the applied force, and this information could be used to foresee how the dislocations should be placed in order to make them interact.

5.3.1 Model 1, two dislocations

In the first model, two screw dislocations were inserted in the slip systems [-111] (101) and [111] (-101). The choice of the dislocations direction and their position in the pillar is made so that it is likely that the dislocations will interact, should they move. Initial tests were also made to make sure that this would be the case. The dislocations are placed with some distance between them so that the dislocations will have to move some distance before interacting, see Figure 5.3.
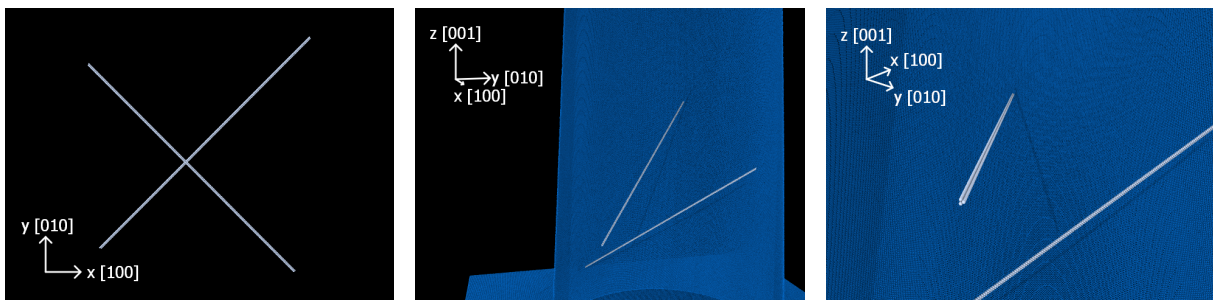
(a) The two dislocations, seen from directly above the pillar.

(b) The two dislocations, seen from the side of the pillar.

(c) Dislocations, seen from the side of the pillar in a slightly different angle.

Figure 5.3: The dislocations that were inserted into Model 1 as seen from different angles of the pillar. All the atoms in the bcc structure is removed and the pillar is cut roughly in half so that only the surface atoms and dislocations as they are seen from inside the pillar are visible.

5.3.2 Model 2, two dislocations

In the second model, the dislocations inserted are the same two as in the first model. That is, the dislocations here as well are positioned in the [-111] (101) and [111] (-101) slip systems. The difference is that these dislocations are positioned much closer together. In fact, the dislocations are so close together that it will later be seen that they are interacting already during the relaxation of the system, and are therefore in contact at the beginning of the compression simulation, see Figure 5.4.
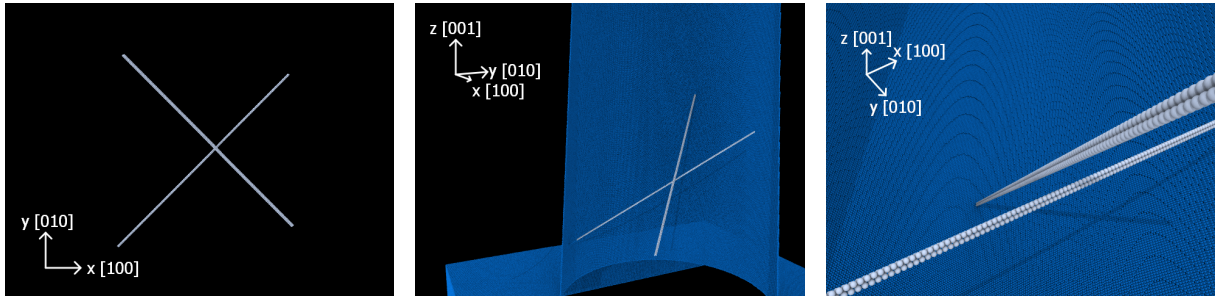
(a) The two dislocations, seen from directly above the pillar.

(b) The two dislocations, seen from the side of the pillar.

(c) The dislocations are initially not in contact as seen from inside the pillar at a different angle.

Figure 5.4: The dislocations that were inserted into Model 2 as seen from different angles of the pillar. All the atoms in the bcc structure is removed and the pillar is cut roughly in half so that only the surface atoms and dislocations as they are seen from inside the pillar are visible.

5.3.3 Model 3, five dislocations

In the third model, the intention has been to insert five dislocations into the pillar in order to simulate how an increased number of dislocations affect the pillar compression. This has been proven not to be so easy. As the program Atomsk is a tool that normally works very well at inserting dislocations, problems with lattice distortion seems to occur more frequently as the number of dislocations increases. This problem did occur already with two dislocations as mentioned in the previous report [1], but it was solved by adjusting the position of the dislocations slightly. It is unclear why this happens and how it can be avoided, but it seems like some combinations of dislocations and their positions create a distortion in the lattice for which the program compensates by deleting atoms creating a line of vacancies. As the number if dislocations increased, it turned out to be very difficult to find a position for the dislocations that did not result in a distorted lattice. The dislocations were therefore positioned neither in order to make them interact, nor randomly, but in the positions which turned out to be successful (without any distortion), see Figure 5.5. Two of the dislocations inserted are approximately the same ones as in Model 1. Unfortunately one of the five dislocations turned out to be positioned in the base directly below the pillar rather in the pillar itself. Therefore the simulation is technically of four dislocations in the pillar though five are inserted in the system. Still it was decided to run simulations on the model as a better alternative was not achieved. It was also seen that though the pillar is clean from any vacancies/debris/deformation, there are some in the pillar base which was not successfully removed. However it is unlikely that this will influence the results in a major way.
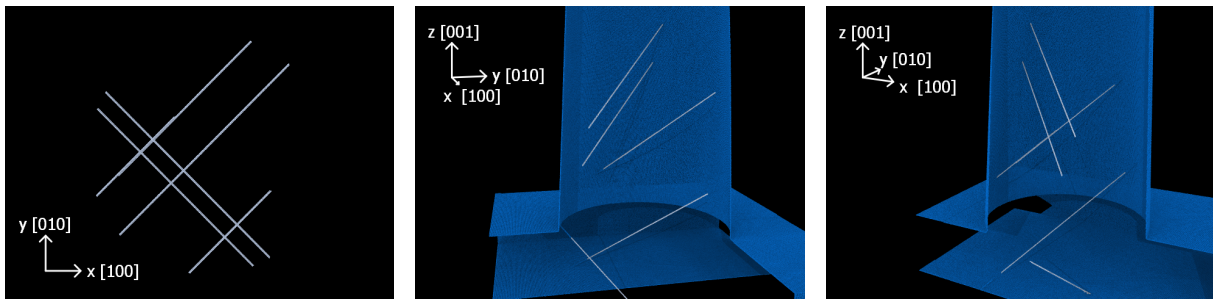
(a) The five dislocations, seen from directly above the pillar.

(b) The five dislocations, seen from the side of the pillar.

(c) The five dislocations, seen from the side of the pillar in a different angle.

Figure 5.5: The dislocations that were inserted into Model 3 as seen from different angles of the pillar. All the atoms in the bcc structure is removed and the pillar is cut roughly in half so that only the surface atoms and dislocations as they are seen from inside the pillar are visible. It can be seen that the 5th dislocation is actually positioned in the base of the model rather than in the pillar itself.

6 | Experimental Procedure

The experimental testing in this thesis was performed on a sample of bcc alpha-Fe with a purity of 99.99%. As the sample previously has been used in other similar experiments, the preparation/polishing of the sample surface had already been done, and a map of the sample surface already existed. For further details on the sample preparation and EBSD analysis procedure, it is recommended to take a look at previous reports written at the faculty/institute [26], [27], and the paper *Strengthening mechanisms of iron micropillars* by Rogne and Thaulow for which this sample was originally prepared [13].

6.1 Fabrication of micropillars

Since the sample is already prepared and ready for testing, the first step in this thesis is pillar fabrication on the iron sample. The premade EBSD plot was used to locate grains corresponding to the crystallographic directions <149> and <235>. These directions as well as the directions <110> and <111> has been used in experimental testing before [26], and further testing of the same directions were therefore of interest. The pillars were manufactured mainly through a three step procedure with an acceleration voltage of 30kV. The procedure is illustrated in Figure 6.1. In order to do compression tests on the pillars later and to get at good visual of the pillar, a wide area around the pillar needs to be cleared. The first step of the procedure is therefore to use high current to mill a circular crater/pit with a diameter of 13 µm around the area where the pillar is to be created. The second step is the milling of the pillar itself inside the crater created in step 1. The third step is the final touch using a relatively low current to straighten the pillar and remove most of the tapering from the previous milling steps. The third step is usually repeated two or three times in order to get a pillar that satisfy the requirement for further testing.
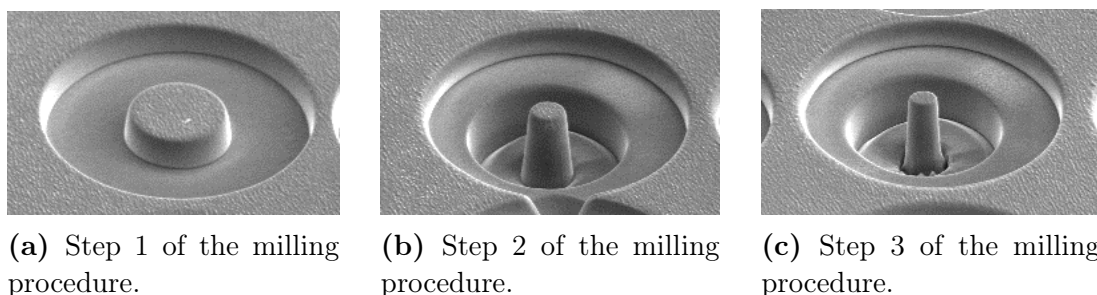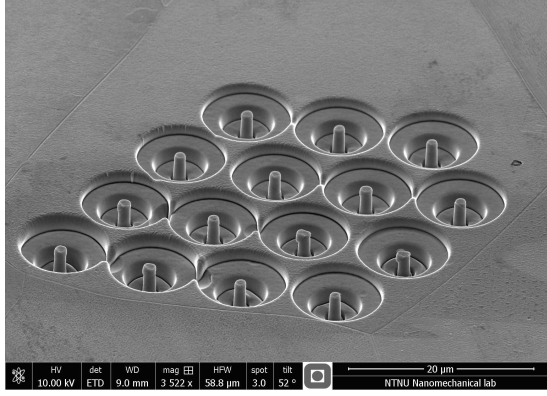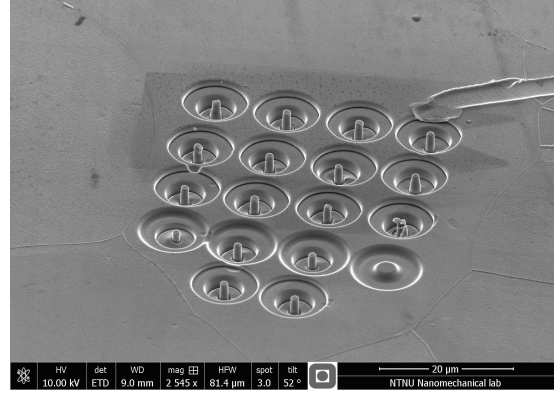

(a) Step 1 of the milling procedure.

(b) Step 2 of the milling procedure.

(c) Step 3 of the milling procedure.

Figure 6.1: The three step milling procedure for making micropillars.

(a) An overview of the dislocations made in the grain with orientation <149>.

(b) An overview of the dislocations made in the grain with orientation <235>.

Figure 6.2: The pictures show all the pillars that were milled in the two chosen grains. Unfortunately the pictures are taken after the indentation of the pillars as there exists no overview pictures of the whole grains prior to testing the pillars.

Figure 6.2 show all the pillars that were fabricated in the chosen two grains with the orientations <149> and <235>. As different grain orientations have different properties, the milling parameters used in the three steps will not necessarily be the same. The parameters used in this thesis are listed in table 6.1. In total, 15 pillars were successfully fabricated in grain <149>, and 16 pillars were successfully fabricated in grain <235>. As some of the pillars fabricated did not meet the standards for further testing, not all of the pillars were used for the final indentation. Some of them were indented during initial testing of the indenter system and cooling equipment instead, prior to beginning with the actual testing.

Table 6.1: FIB milling parameters for creation of pillars with <149> and <235> orientation.

|	Step 1	Step 2	Step 3
Orientation <149>, 15 pillars			
Outer diameter [µm]	10	6	2.3-2.4
Inner diameter [µm]	4	1.5	1.2
z [µm]	0.35-0.4	0.45	0.1
Current	2.7nA	90pA	26pA
Orientation <235>, 16 pillars			
Outer diameter [µm]	10	6	2.0-2.2
Inner diameter [µm]	4	1.5	1.2
z [µm]	0.6	0.8	0.1
Current	2.7nA	90pA	26pA

6.1.1 Discarded pillars

A few of the pillars that were made had to be discarded due to various fault and mistakes made during the fabrication process. A problem that revealed itself for the first pillars made was drift of the ion beam as it was a relatively long time since the last maintenance of the FIB. The drift was not large enough to be visible when adjusting the focus of the beam and making the milling pattern, but as the second milling step could take as long as 15-20 minutes, this affected the milling of the pillars and made them askew. There was performed maintenance on the FIB before the next sessions, and the drift experienced was very small after that.

It also became a problem one session that the pillars produced did not have well defined edges, and that the top of the pillar itself became unusually thin. This turned out to be a novice mistake as it had not been taken care to adjust the focus of the ion beam when moving to different vertical positions on the tilted sample. This had a large effect on the outcome of the milling process, and some of the pillars produced could not be used in further testing.

A third reason for why some pillars were discarded was the occasional presence of impurities or grain boundaries beneath the surface. This resulted in different hardness/orientations in some parts of the pillars which destroyed the final result.
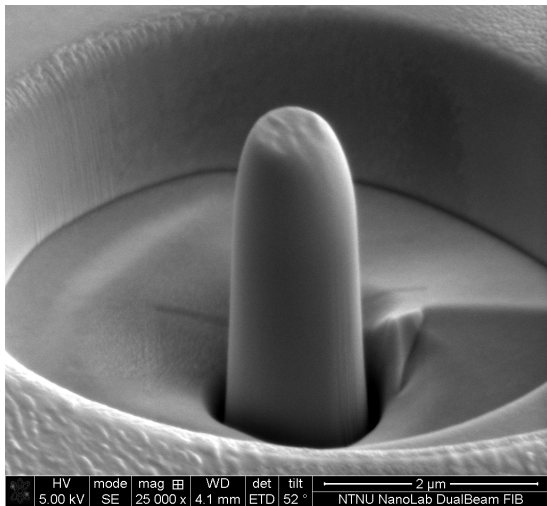
(a) The ion beam was not properly focused, which lead to the edges of the pillars being very diffuse.
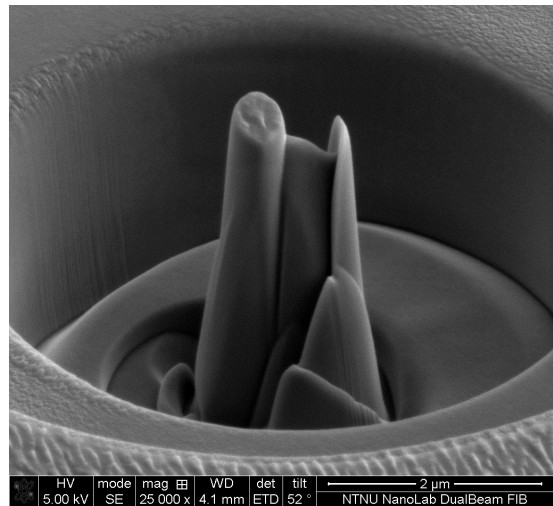
(b) Possible impurities or grain boundaries beneath the surface of the sample lead the pillar to be unevenly milled and destroyed.

**Figure 6.3:** Some pillars did not turn out as intended and had to be discarded.

6.2 Indenting process

The equipment used to perform compression tests on the micropillars was a Hysitron PI 85 Picoindenter supplied with a TriboScan software at the Nanomechanical lab at IPM, NTNU. The picoindenter was installed inside the SEM vacuum chamber and the stage was positioned so that the indenter tip was as close to the two grains as possible in the x- and y-directions, as the indenter probe has limited movement in these directions after being mounted.

Approximately half of the pillars in each grain were indented at room temperature. After all the chosen pillars were indented, the cooling system recently developed at NTNU by other master students were installed and both the sample and the indenter tip was cooled down to -80°C. After reaching the right temperature the rest of the pillars in the two grains were indented. The indentation was performed in an open-loop load control mode. The displacement and load of the indenter tip was recorded for each indentation and converted to stress-strain curves. Pictures were also taken for each of the pillars in order to later be able to perform slip trace analysis of the indented pillars. No slip trace analysis was performed for this thesis though, as the equipment used to take the final pictures was frequently down for maintenance due to malfunctions the last few weeks. The pictures were therefore acquired at a very late stage in the project work, leaving no time for further analysis.

Figure 6.4: Picture of the indenter equipment installed in the SEM [26]
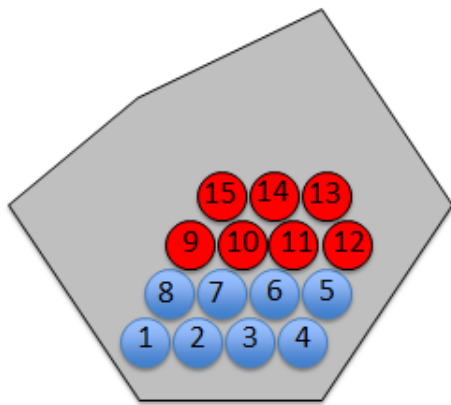
(a) A sketch of the grain with <149>-orientation, including the numbering corresponding to the positions of the pillars in the grain
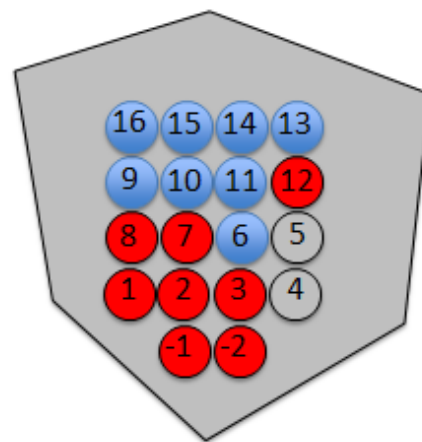
(b) A sketch of the grain with <235>-orientation, including the numbering corresponding to the positions of the pillars in the grain.

Figure 6.5: Illustraion of the pillar positions in the <149>- and <235>-oriented grains. The pillars coloured red were indented at room temperature. The pillars coloured blue were indented at -80°C. The pillars corresponding to the position of the grey circles were never finished/destroyed during milling.

Part III

Results

7 | Strain rate

7.1 Effect of strain rate on yield stress

As it was decided during the project that running simulations at a lower strain rate was of interest, it also became interesting to actually examine the effect different strain rates would have on the simulation results. The strain rate is often one of the main limitations of atomistic simulations, as even supercomputers does not have the capacity to do the huge amount of calculations required to perform the simulations over a realistic time period. Six simulations of six different strain rates were run on a pillar model with no initial dislocations and at a temperature of 300K. The results are illustrated inn Figure 7.1
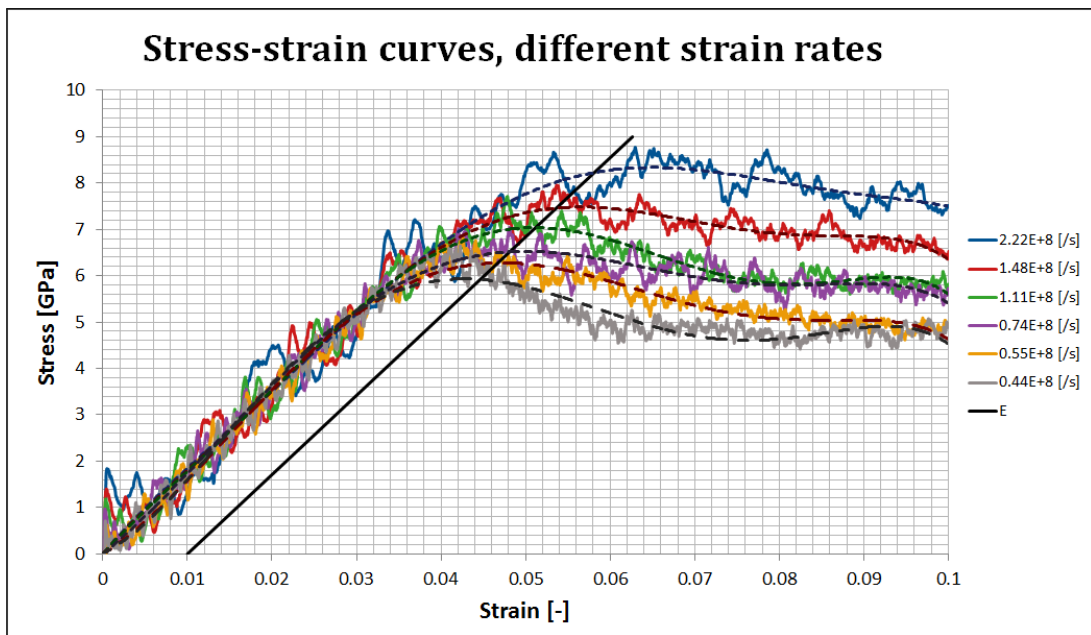

Figure 7.1: The graph shows the stress-strain curves for simulations of six different strain rates between $0.44 \cdot 10^8 s^{-1}$ and $2.22 \cdot 10^8 s^{-1}$. The line of the E modulus at 1% offset, calculated as the mean of the measured E modulus of all the curves, is included in the plot.

The resulting stress-strain curves showed a strong coherence between the strain rate and the yield stress of the pillar. The highest strain rate seemed to have the highest yield stress, with decreasing yield stress for decreasing strain rate. Excluding the graph with the highest strain rate because the variations were to big to get a good measurement, the E modulus for each simulation was estimated to be between 168-172GPa, with consistently increasing E modulus for decreasing strain rate. A mean value of 171GPa was chosen and the line of the E modulus with a 1% offset was drawn in the graph together with

the stress-strain curves. A trend line was made for each of the graphs with a 6th order polynomial fitting which was the best one available in Excel. These are also included in the plot. For the high strain rates, the 1% offset yield stress was measured from the trend lines included in the graph. For the two lowest strain rates, new trend lines for a smaller part of the curve close to the yield point was made in order to measure a more accurate yield stress. The yield stresses acquired from the results in Figure 7.1 were then plotted against their strain rate in Figure 7.2.
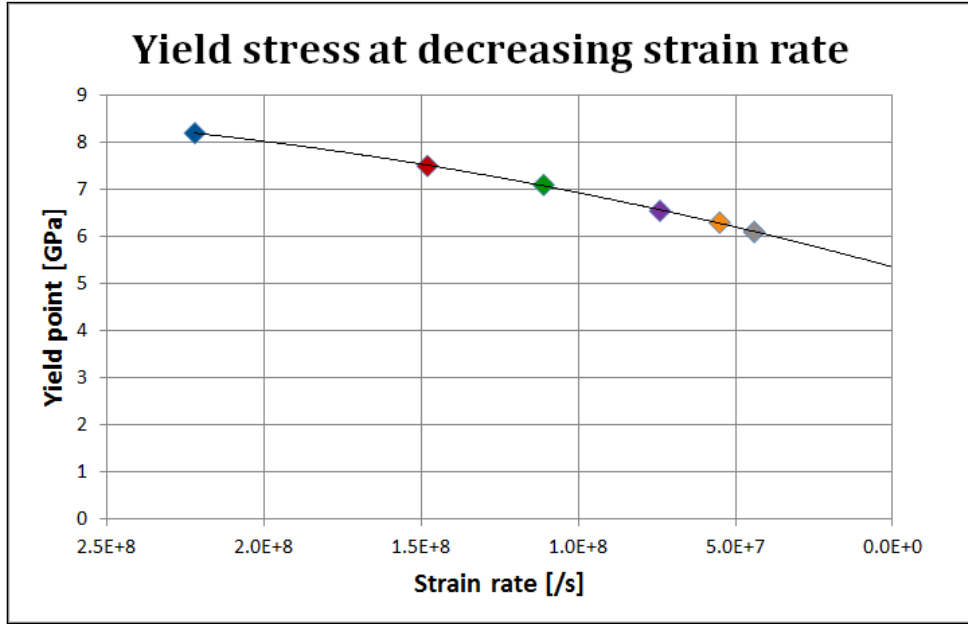

Figure 7.2: The graph shows the yield stress of the curves illustrated in Figure 7.1 as a fuction of the strain rate for which they were aquired. The yield stress was measured at a 1% offset. The curve fitting used to find a relation between the plotted yield points is a simple 2nd order polynomial one.

The graph in Figure 7.2 showed a remarkable clear relation between the yield stress and the strain rate, considering the few measuring points and the sources of error that might occur when reading a value from the trend line of a stress-strain curve. The points plotted showed a clear tendency corresponding well to a simple 2nd order polynomial trend line. A normal strain rate for experimental testing is in the order of magnitude 10^{-3} which in this plot is very close to zero. By extrapolation of the trend line, it can safely be assumed that strain rate plays an important part in the reason why simulations show much higher stresses than experimental testing. Just for these few measure points, the yield stress was decreased from 8.2GPa at $2.22 \cdot 10^8 s^{-1}$ to an estimated 5.4GPa at a "normal" strain rate. This is the case if we assume the yield stress follows the trend line plotted. In reality there are too few measure points at low strain rate to actually conclude that this trend line shows the real coherence, as the curve might take a different shape as she strain rate decreases further.

$$\frac{\tau^*}{\tau^*(0K)} = \left[1 - \left\{ -\frac{kT}{G_0^*} ln(\frac{\dot{\epsilon_\tau}}{\dot{\epsilon_0}}) \right\}^{\frac{1}{q}} \right]^{\frac{1}{p}} \qquad (2.8)$$

Equation 2.8 has previously been suggested as a possible relation between strain rate and shear stress. If one assumes that a similar relation exists between strain rate and yield stress, this equation could be used to predict the change in yield stress from the strain rate used in the simulations and the strain rate used in the experimental testing. The value for $\tau^*(0K)$ was changed to 6900MPa which is the approximate yield stress corresponding with the value for $\dot{\epsilon}_0 = 1 \cdot 10^8 s^{-1}$ from Figure 7.2. The temperature T was set to 300K and the rest of the constants were kept the same as in the original equation. Equation 2.8 was then plotted together with the measured yield stresses and their estimated trend line in a logarithmic plot. The result is showed in Figure 7.3. In this case it can be seen that the yield is estimated to decrease much more, down to approximately 500MPa. This value is somewhat low compared to values from the expected values previously illustrated in Figure 2.4. It is very possible that there is a relation that could be expressed by a similar equation, but with some slight changes. As the stresses acquired from Equation 2.8 also did diverge some from the ones acquired from simulations, some plots were made with different values for $\dot{\epsilon}_0$, q and p. Some of these plots fitted the simulated values much better, but affected the rest of the curve a lot. The estimated yield stresses at $1 \cdot 10^{-3}$ strain rate could vary from 0 to 3500MPa and still fit the values from the simulations pretty well. With this in mind it can be assumed that the equation 2.8 is very close to showing the dependence of the strain rate on the simulated stresses, but there exists too few measure points from simulations at relatively low strain rates to draw a good and exact conclusion.
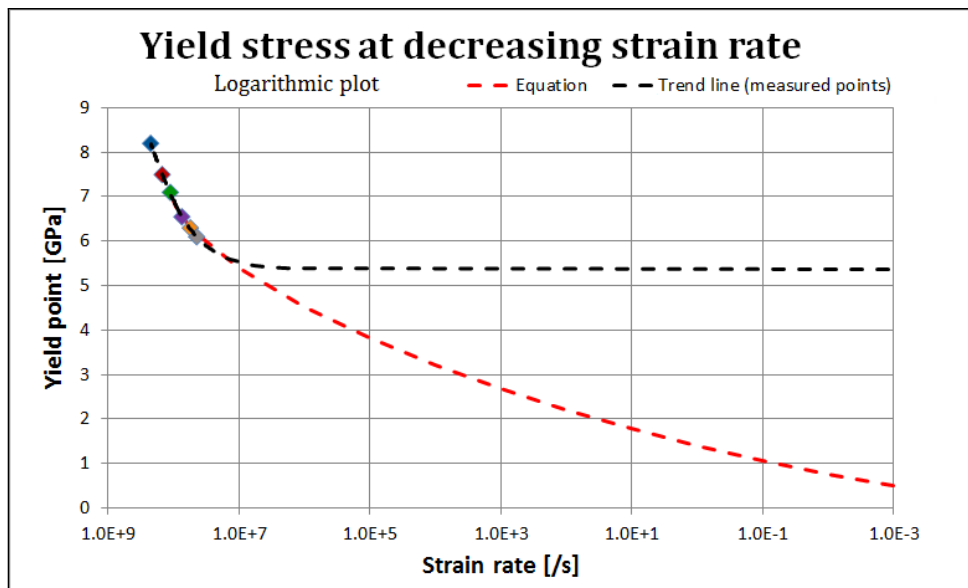

Figure 7.3: The logarithmic plot of the curve from Figure 7.2. The graph also includes the logarithmic plot of Equation 2.8 with parameters adjusted for the measured points from the simulations.

8 | Simulation results

8.1 Stress-strain curves

As the simulations are running, the force on the indenter and the indenter position are recorded for each 200th time step. This information is used to make stress-strain curves for the compression performed on the pillars. The yield stress for all the curves, measured at 1% offset, is listed in Table 8.1. Also included in the table is the stress value registered at the moment new dislocations, not related to the initial ones inserted into the pillar, appears. These new dislocations appear as mixed dislocations (edge dislocation front, and screw dislocation sides with mixed sections in between) at the base of the pillar as a precursor to the approaching yield. Detailed analysis of these new dislocations and the deformation following the yield have not been performed as it has not been one of the main focuses of this thesis. The topic has been covered in similar simulations carried out at NTNU previously [15].

Table 8.1: The yield stress measured at 1% offset for all the simulations, with both strain rates and temperatures. Also included are the stress values for which the first dislocations *other* than the ones initially inserted appear from the base of the pillars.

	$3.33 \cdot 10^8[/s]$		$0.74 \cdot 10^8[/s]$	
	First dislocation	0.1% offset yield	First dislocation	0.1% offset yield
15K	6.49	11.1	7.07	8.2
15K M-1	6.46	11.0	6.06	7.6
15K M-2	6.41	11.0	6.02	7.5
15K M-3			5.98	7.5
300K	6.43	9.3	6.25	6.5
300K M-1	6.69	9.5	4.88	6.7
300K M-2	6.68	9.5	5.80	6.75
300K M-3			5.11	6.5

High strain rate

For the highest strain rate, $3.33 \cdot 10^8 s^{-1}$, simulations were run for Model 1, Model 2 and a pillar with no initial dislocations. The stress-strain curves from these simulations are illustrated in Figures 8.1 and 8.2. At this point, Model 3 was not developed yet. In general, the curves acquired from these simulations shows great fluctuations which can not be related to specific mechanisms observed in the simulations themselves. These fluctuations were the main reason for the decision to run a new round of simulations, as the high strain rate is believed to be the main reason behind them. It was also observed a rapid increase in stress almost immediately as the simulations starts. The simulations are

displacement controlled and the indenter had initially constant velocity throughout the whole simulations. This is believed to be the cause behind the rapid increase in stress as the indenter basically collides with the pillar surface with a constant velocity, and the material needs some time to respond elastically to the pressure. A new section was therefore added to the simulation script in order to increase the velocity of the indenter gradually up to the preset constant value used for the main part of the simulations.Apart from these sources of error, it can be observed for the high strain rate that the stress-strain curves show slightly different behaviour at the different temperatures. While the simulations run at room temperature shows a yield stress of roughly 9.5GPa, the yield stress at low temperature is closer to 11GPa. It also seems like the stress-strain curve for the higher temperature fluctuates slightly more. This corresponds well with the anticipated temperature dependency of the mechanical properties. Interestingly, almost immediately after reaching yield, the stress-strain curves at 300K temperature drops suddenly to approximately half the stress value. The stress drops after yield for the 15K curves as well but not as much and not as rapidly.

Low strain rate
For the relatively low strain rate, $0.74 \cdot 10^8 s^{-1}$, simulations were run for Model 1, Model 2, Model 3 and a pillar with no initial dislocations. The stress-strain curves from these simulations are illustrated in Figures 8.3 and 8.4. In comparison with the curves from the high strain rate, these curves have very little fluctuations. The fluctuation that still are visible in the curves at low strain rate is noticeably more even and seemingly periodic, which makes it likely that they are the result of normal oscillations in the system environment. The decision to lower the strain rate and to include an initial ramping of the indenter velocity does therefore seem to have achieved much more accurate simulations and stress-strain curves. Also here it seems like the fluctuations are slightly higher for the higher temperature, which corresponds well with previous assumptions. As for the stress-strain curves with higher strain rate, the low temperature curves show a higher yield strength than the room temperature ones with approximately 7.5GPa for low temperature to 6.7GPa for room temperature. The drop in stress after yield in much less than for the higher strain rate, but here as well the curves at room temperature seem to drop slightly more than the curves for the low temperature which stays at approximately the same stress value. However, an interestingly observation is that as the stress is starting to stabilise from the drop after yield, it seems to stabilise at approximately 7-8Gpa at 15K temperature and approximately 4-6GPa at 300K temperature for *both* the strain rates, Figures 8.1 - 8.4. As if the drop in stress after yield is compensating for the increased tress caused by the higher strain rate.
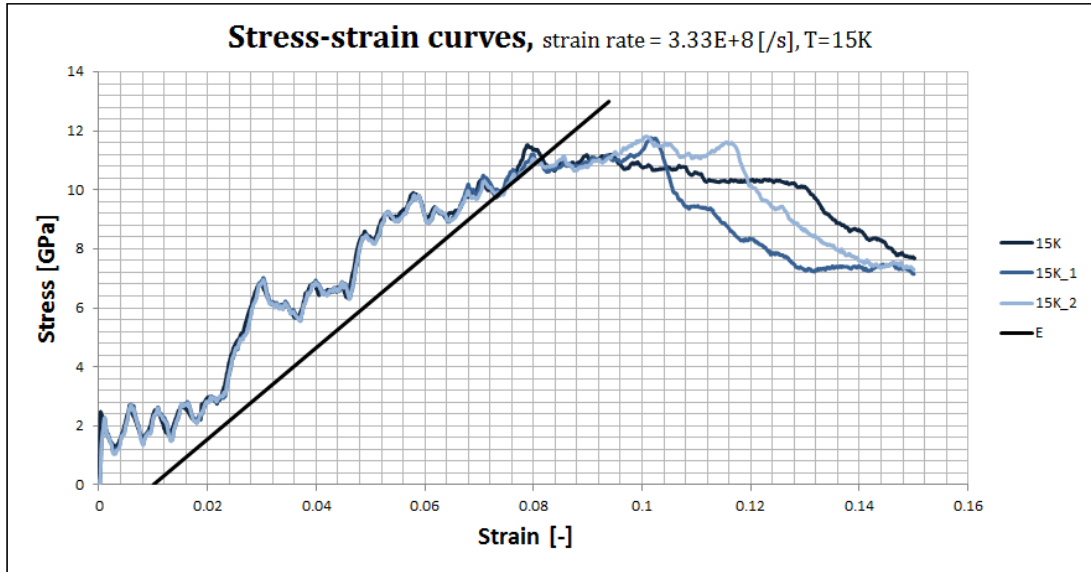
Figure 8.1: Stress-strain curves for the simulations with temperature 15K and with strain rate $3.33 \cdot 10^8 s^{-1}$. Pillar Model 1, Model 2 and a pillar without any initial dislocations were simulated at this low temperature and high strain rate. The line used to measure 1% offset yield based on the calculated E modulus is also included.
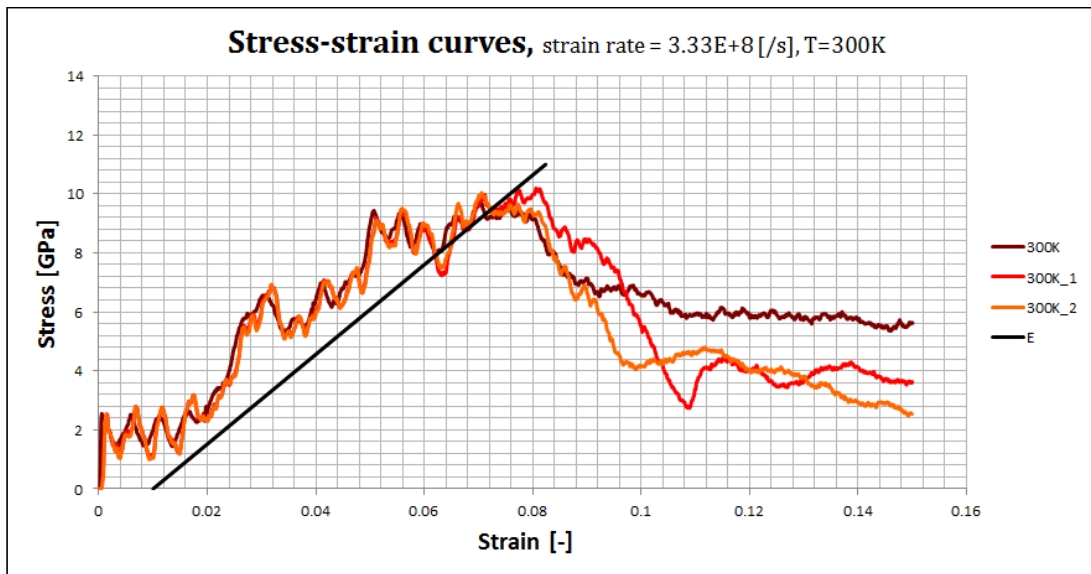

Figure 8.2: Stress-strain curves for the simulations with temperature 300K and with strain rate $3.33 \cdot 10^8 s^{-1}$. Pillar Model 1, Model 2 and a pillar without any initial dislocations were simulated at room temperature and with high strain rate. The line used to measure 1% offset yield based on the calculated E modulus is also included.
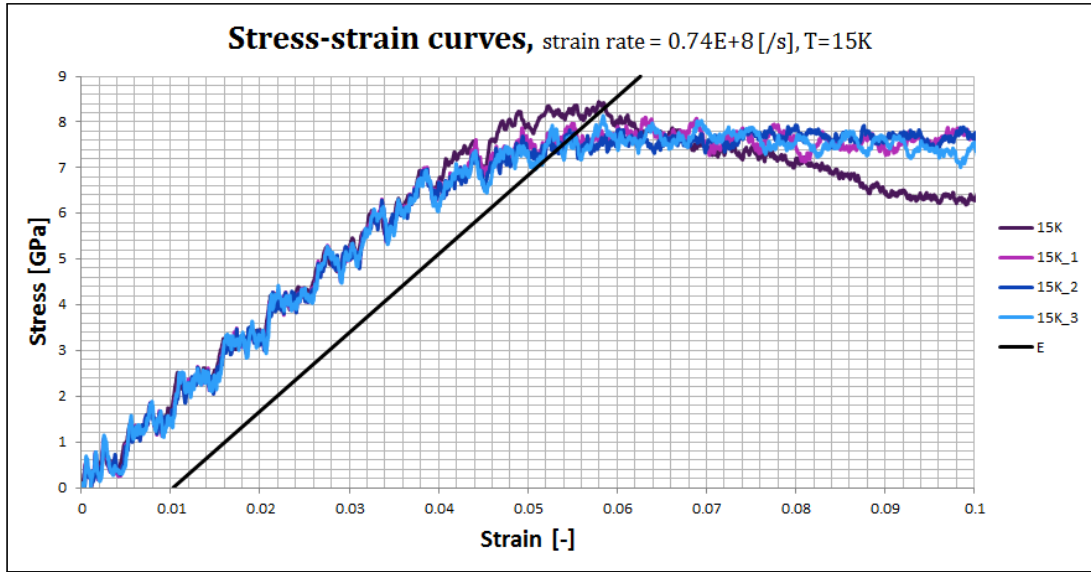
Figure 8.3: Stress-strain curves for the simulations with temperature 15K and with strain rate $0.74 \cdot 10^8 s^{-1}$. Pillar Model 1, Model 2, Model 3 and a pillar without any initial dislocations were simulated at this low temperature and relatively low strain rate. The line used to measure 1% offset yield based on the calculated E modulus is also included.
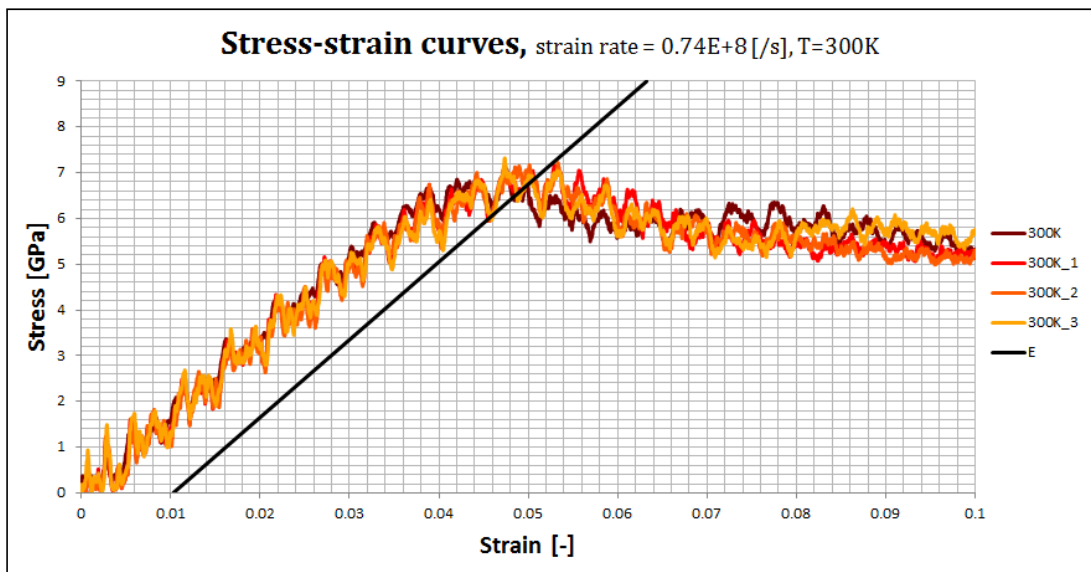

Figure 8.4: Stress-strain curves for the simulations with temperature 300K and with strain rate $0.74 \cdot 10^8 s^{-1}$. Pillar Model 1, Model 2, Model 3 and a pillar without any initial dislocations were simulated at room temperature and with relatively low strain rate. The line used to measure 1% offset yield based on the calculated E modulus is also included.

Modulus of elasticity

A clear tendency that was observed was the change in the value for the E modulus depending on strain rate and temperature. As mentioned in the previous chapter, the E modulus decreases for increasing strain rate. For the low temperature curves, the E modulus increased from 155GPa to 172GPa as the strain rate was decreased. For the room temperature curves, the E modulus increased from 152GPa to 170GPa. Therefore it was also evident that the E modulus was slightly lower for higher temperatures.

Number of dislocations

The stress-strain curves acquired for Model 1, 2 and 3 simulated under the same conditions, are very similar. There are no clear differences/patterns in the curves which could indicate different mechanical properties depending on the number of dislocations and their positions. However, for all the four combinations of temperature and strain rate, the simulation with no initial dislocations stand out. The fluctuations in the curves resulting from the simulations with no initial dislocations seems to have a slightly smaller amplitude, which is seen most clearly at the elevated temperatures. For the high strain rate curves, no trends depending on the initial dislocations is observed close to the yield point, other than that the yield stress is slightly lower at 300K and slightly higher at 15K for the pillar with no initial dislocations, but this could be just a coincidence. After yield though, the stress does not drop as much for the pillar with no dislocations as it does for the two others. For the simulations with low strain rate, the pillar with no initial dislocations also shows a slight tendency to have a lower yield point rather than a drop in stress after yield. For the same case with low temperature however, the curve for the pillar with no dislocations takes off along its own path as it gets close to yield. Its yield stress it noticeably higher, and the stress decreases rapidly thereafter.

8.2 Simulations with a temperature of 15K

In the previous project work leading up to this thesis [1], it was a general problem that the dislocations inserted in the pillars had a tendency to leave the pillars during the relaxation part of the simulation. This was believed to be due to mirror stresses acting on the dislocation. Due to the circular geometry of the pillar and the small diameter, the dislocations were able to effectively decrease their total length a lot by moving small distances in the pillar. Therefore it was energetically favorable for the dislocations to leave the pillars as quickly as possible. Though these new simulations feature much larger pillars, it was surprisingly observed that *none* of the dislocations left the system during the relaxation. In fact, apart from small movements where one of the end points of the dislocation line changes position a few Å in order to stabilise the dislocation in a more natural position, the dislocations have not moved at all during the relaxation. In this section, some pictures of the dislocations inside the pillar models during the simulations at the temperature 15K will be presented.

In order to see the movement of the dislocations more clearly, all atoms in the simulations having a BCC structure have been deleted for the visualisation of the following pictures. The atoms of the pillar surface have been coloured blue, and the atoms belonging to the dislocations have been coloured white. Half of the pillar surface have also been removed in order to be able to see the inside of the pillar.

8.2.1 15K - Model 1

For the simulations of Model 1 at the temperature 15K, both dislocations are after the relaxation positioned with some distance between them as they were initially inserted. For the pillar simulated at low strain rate, the dislocations start to move shortly after the compression of the pillar starts. The movement is however relatively slow. At 0.0084 strain, the two dislocations come in contact and merge as seen in Figure 8.5. At the point where the pillar starts to experience yield, the dislocations are still in contact and have visibly not moved at all since they first connected. By stating that the dislocations have not moved, what is meant is that the points where the dislocation lines are ending in the pillar surface are the same, as if the dislocations are locked in place at the surface. The dislocation line itself is moving frequently in partially sharp movements as illustrated by an example in Figure 8.6, where what is believed to be a kink travels along the dislocation line. The point at the stress-strain curves corresponding to the time steps for which the pictures are taken is illustrated in Figure 8.8.

For the pillar simulated at high strain rate, the two initial dislocations barely move along the pillar surface at all except for the slight adjustment done during the relaxation. Instead, the end points of the dislocations are pinned to the surface, while what appears to be two kinks are travelling back and forth along the dislocation line leaving behind what appears to be close to pure screw segments. This is illustrated in Figure 8.7. At the point where the pictures are taken, dislocations have started to initiate from the base of the pillar, but it can be seen that the dislocations still haven't moved much. The points at the stress-strain curve which corresponds to the time steps for which these pictures are taken are illustrated in Figure 8.9.
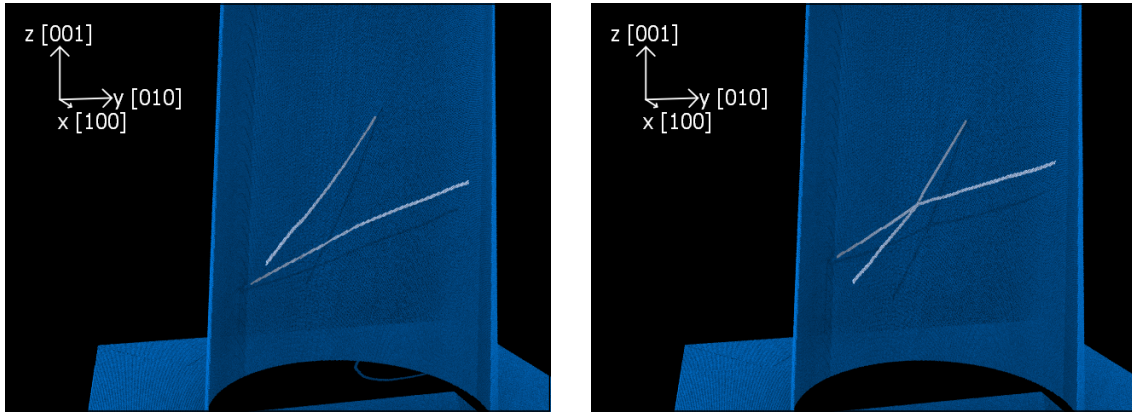
(a) The position of the dislocations at $\epsilon = 0$, after the relaxation.

(b) The dislocations have made contact and merged at $\epsilon = 0.0084$

Figure 8.5: The movement of the dislocations inside Pillar Model 1 during the simulation with temperature 15K and low strain rate.
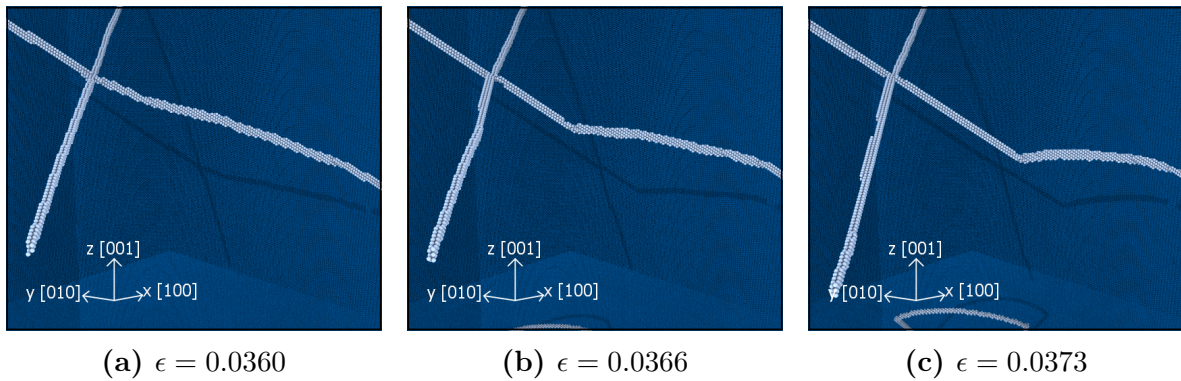

(a) $\epsilon = 0.0360$

(b) $\epsilon = 0.0366$

(c) $\epsilon = 0.0373$

Figure 8.6: Dislocation movement observed for Pillar Model 1 at low temperature and low strain rate. After the two screw dislocations merge, the mixed segments of one of the original screw dislocations creates what is most likely a kink, travelling along the dislocation line, leaving behind a pure screw segment.
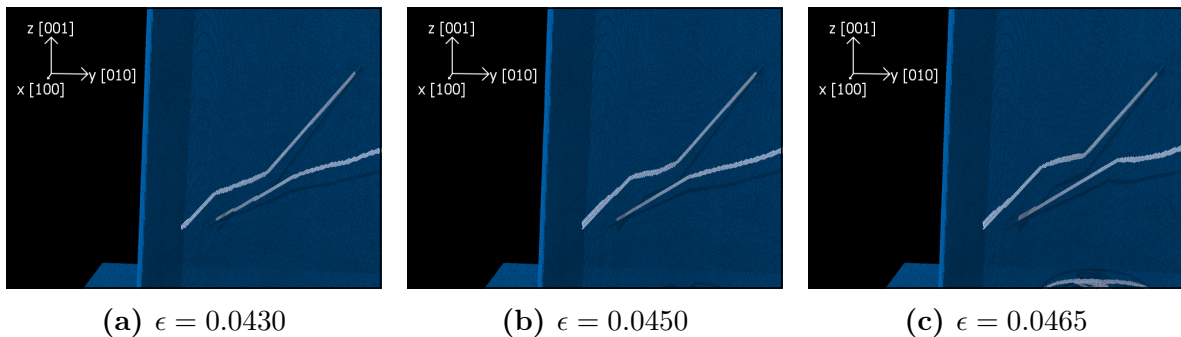

(a) $\epsilon = 0.0430$

(b) $\epsilon = 0.0450$

(c) $\epsilon = 0.0465$

Figure 8.7: Dislocation movement observed for Pillar Model 1 at low temperature and high strain rate. What appears to be two kinks are created on the dislocation line, travelling back and forth between the two points where the dislocation ends in the surface.
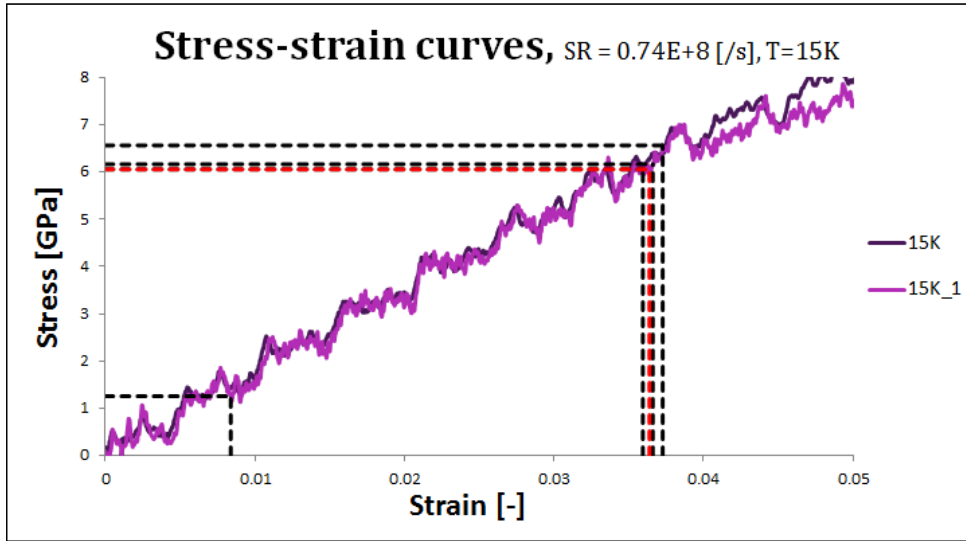
Figure 8.8: The stress strain curve of Model 1 and the pillar with no initial dislocations at low strain rate and low temperature. The red line indicated the point where the first dislocations appear from the base of the pillar. The black lines are the time steps of the simulation corresponding to the pictures in Figures 8.5b and 8.6.
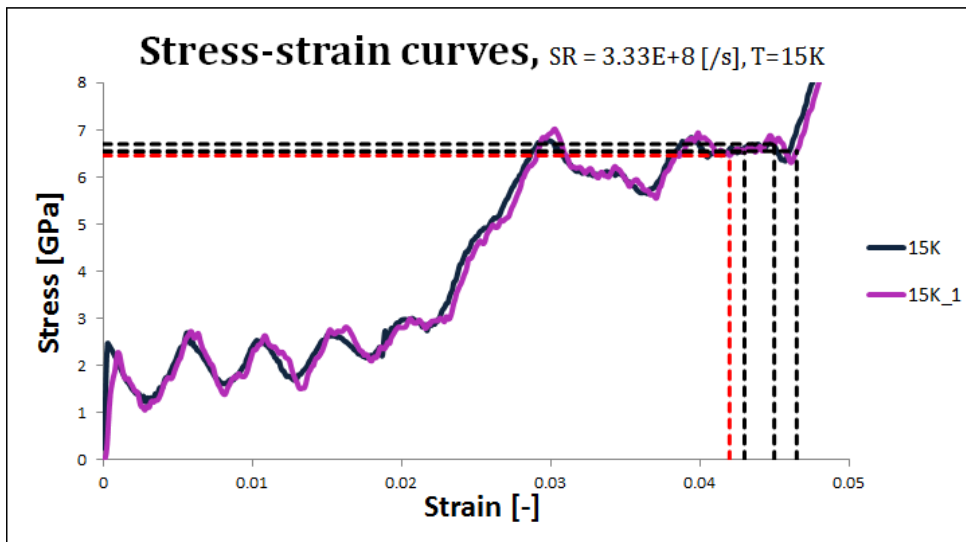

Figure 8.9: The stress strain curve of Model 1 and the pillar with no initial dislocations at high strain rate and low temperature. The red line indicated the point where the first dislocations appear from the base of the pillar. The black lines are the time steps of the simulation corresponding to the pictures in Figure 8.7.

8.2.2   15K - Model 2

For the simulations of Model 2 at the temperature 15K, the dislocations are initially positioned so close together, that they make contact and merge during the relaxation of the system. For the pillar that was simulated with low strain rate, the dislocations start to move slowly together very early in the simulation. It can be seen though from Figure 8.10, that the dislocations does not really manage to move that far at all before the new dislocations start to appear shortly after the picture in Figure 8.10b is taken, which is illustrated in Figure 8.11. The movement that is observed seem to occur by kink segments similar to the ones described before, which in this case reposition the dislocation line when they reach the surface of the pillar. It can also be seen that intersection between the two dislocations have left behind some debris in its path.
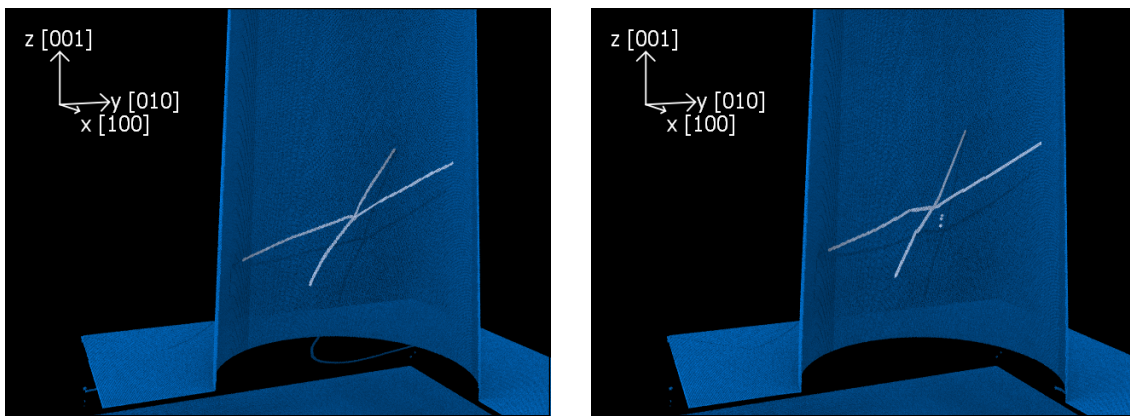
(a) The position of the dislocations at $\epsilon = 0$, after the relaxation.

(b) The picture taken at $\epsilon = 0.0357$ shows that the dislocations have barely moved.

Figure 8.10: The movement of the dislocations inside Pillar Model 1 during the simulation with temperature 15K and low strain rate. The dislocations have barely moved, though left behind some debris in their path, before the creation of new dislocations from the base of the pillar a few time steps later.

For the corresponding simulation at high strain rate, the situation is very much the same, but it does not leave behind visible debris. Here as well, the two dislocations starts to slowly move upwards in the pillar, before new dislocations are created and yield occurs. The presence of kink segments might be slightly more protruding at the high strain rate than at the low strain rate, but otherwise the dislocation behaviour for the two simulations are very similar.
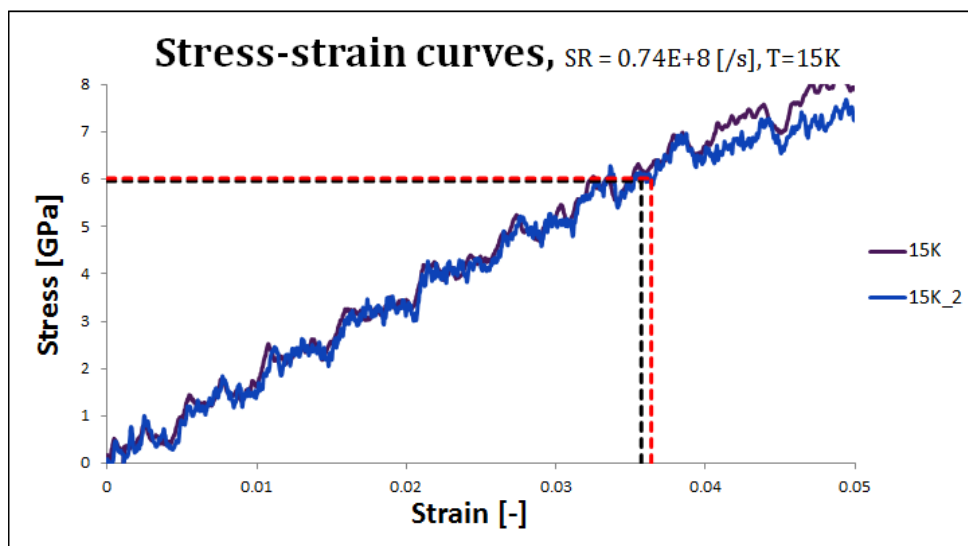
Figure 8.11: The stress strain curve of Model 2 and the pillar with no initial dislocations at low strain rate and low temperature. The red line indicates the point where the first dislocations appear from the base of the pillar. The black line is the time step of the simulation corresponding to the picture in Figure 8.10b.

8.2.3   15K - Model 3

Model 3 was only simulated at the low strain rate. For the simulations of the model at the temperature 15K, there are five dislocations inside the model as the compression starts. Two of these dislocations are very much the same ones as were simulated for Model 1, and it can be seen that these are also the ones that start to interact at 0.0064 strain as seen in Figure 8.13b. These two dislocations merge and keep together until 0.0355 strain is reached, at which point they separate again. Interestingly, the top left dislocation of these two (The one with its dislocation line in the <-111> direction as illustrated in 8.13), is the one moving down in order to interact with the other dislocation, as well a being the one that tears away and travels upwards later on. Except for these two dislocations, the others does not move much until yield is reached. The top dislocation slowly moves a some distance upwards and the one of the two lower dislocations with a dislocation line in the <111>-direction move slightly downwards. The last dislocation is pinned in the same position and does not seem to move. All the dislocations are still present in the pillar as yield is reached. It can be noted that the two dislocations that interact are the only ones at 15K which has enough energy to both merge *and* separate before yield. For all the other simulations with temperature 15K, the dislocation have either merged and stayed together that way, or they have not had enough energy to interact at all. The points at the stress-strain curve corresponding to the time steps for which these pictures are taken are illustrated in Figure 8.12.
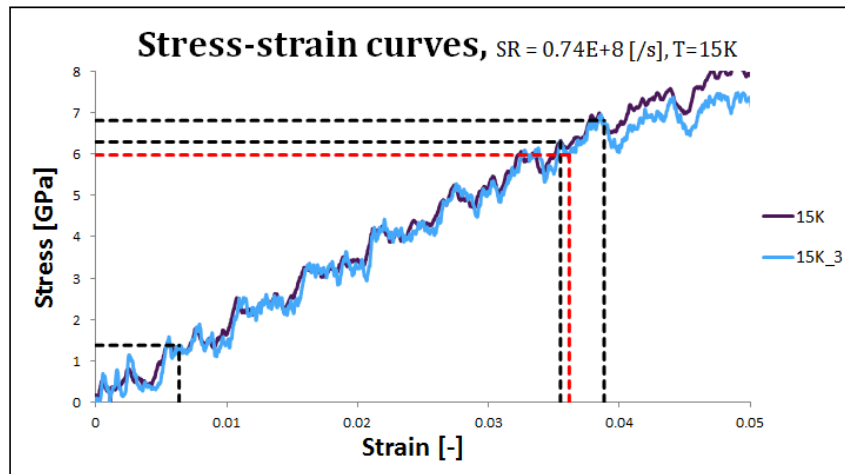

Figure 8.12: The stress strain curve of Model 3 and the pillar with no initial dislocations at low strain rate and low temperature. The red line indicates the point where the first dislocations appear from the base of the pillar. The black lines are the time steps of the simulation corresponding to the pictures in Figure 8.13
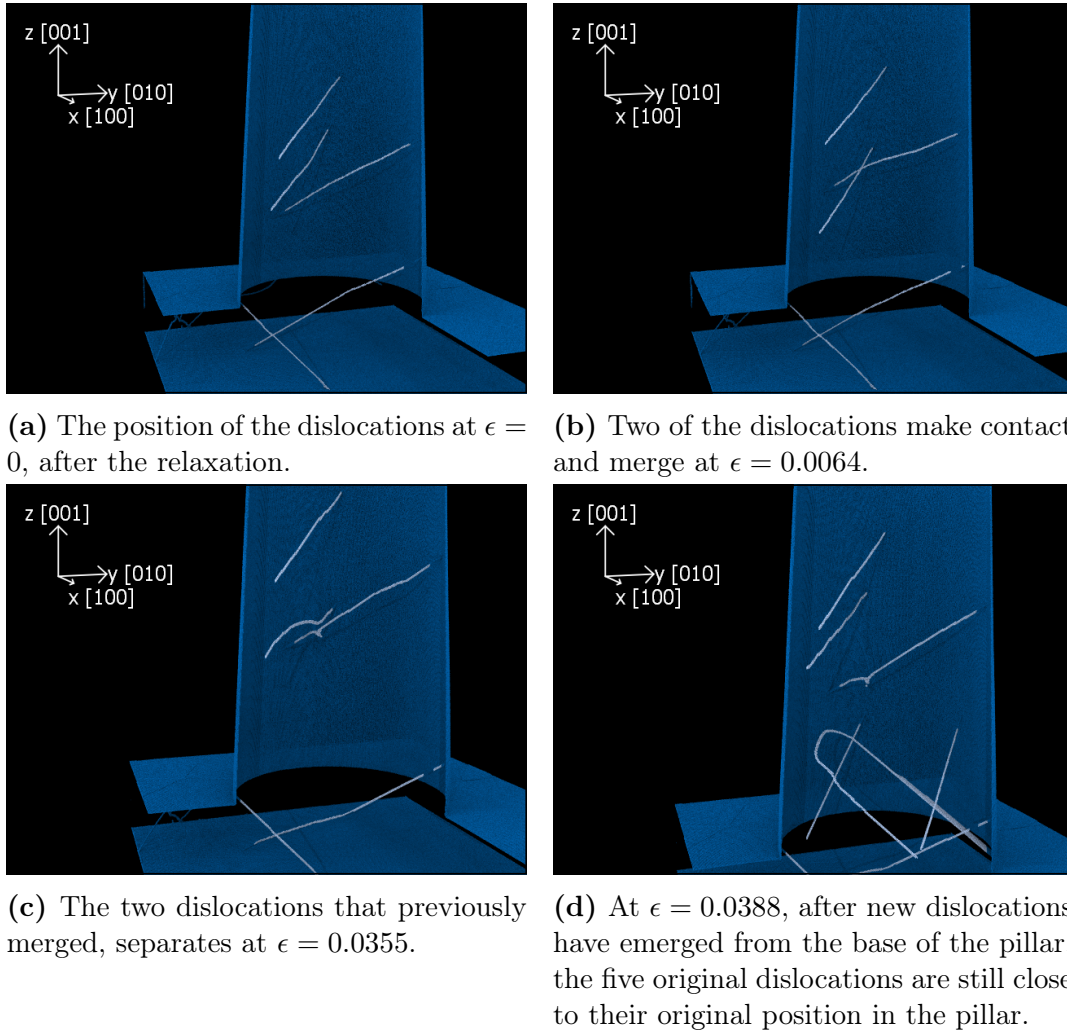
(a) The position of the dislocations at $\epsilon = 0$, after the relaxation.

(b) Two of the dislocations make contact and merge at $\epsilon = 0.0064$.

(c) The two dislocations that previously merged, separates at $\epsilon = 0.0355$.

(d) At $\epsilon = 0.0388$, after new dislocations have emerged from the base of the pillar, the five original dislocations are still close to their original position in the pillar.

Figure 8.13: The movement of the dislocations inside Pillar Model 3 during the simulation with temperature 15K and low strain rate. All the dislocations are still present when approaching the yield stress.

8.3 Simulations with a temperature of 300K

For the simulations at a temperature of 300K, one would believe that there was a higher risk of the dislocations moving a lot and disappearing from the pillar during the relaxation of the system. Though the dislocation have moved slightly to adjust themselves during the relaxation, they are still observed to be positioned very close to the same position as they were originally inserted. At 300K temperature, the dislocations generally move in a different way than they did at 15K. Where the movements of the dislocations at low temperature were sort of stepwise and angular , and seemed to be driven by creation and movement of kinks, the dislocations at higher temperature moved more smoothly, forming circles and small loops rather than sharp edges and straight lines.

8.3.1 300K - Model 1

For the simulations of Model 1 at the temperature 300K and high strain rate, the dislocations start to move towards each other as soon at the compression of the pillar starts. As seen in Figure 8.14 they make contact at 0.02 strain, but the dislocation which originally had a dislocation line in the <111> direction and was positioned below the other, does not stop its upward movement. The dislocation keeps moving upwards, also moving the intersection point of the two dislocations upwards. Shortly after initiation of new dislocations, Figure 8.14c and Figure 8.16, this dislocation starts to form a large loop while still connected to the other dislocation. Eventually this loop increases until it reaches the pillar surface, at which point it splits into three dislocations. Though at this point in the simulation, yield has occurred.

For the simulation with low strain rate, the dislocations have made contact at 0.0059 strain as seen in Figure 8.15b. The dislocations are connected for quite some time, choosing to move upwards together rather than separating. The lower part of the dislocations move slightly faster than the upper ones, making the dislocation lines take on a more horizontal appearance with some mildly circular sections formed by mixed dislocations. The two dislocations separate at 0.0268 strain, Figure 8.15c. The dislocation that initially had a dislocation line in the <111> direction leave the pillar right before new dislocations emerge, while the other one leaves shortly thereafter. The points at the stress-strain curve corresponding to the time steps for which these pictures are taken, are illustrated in Figure 8.17.
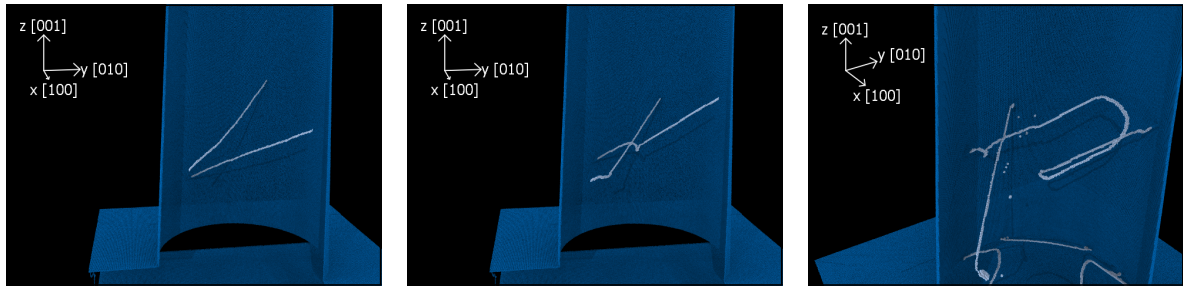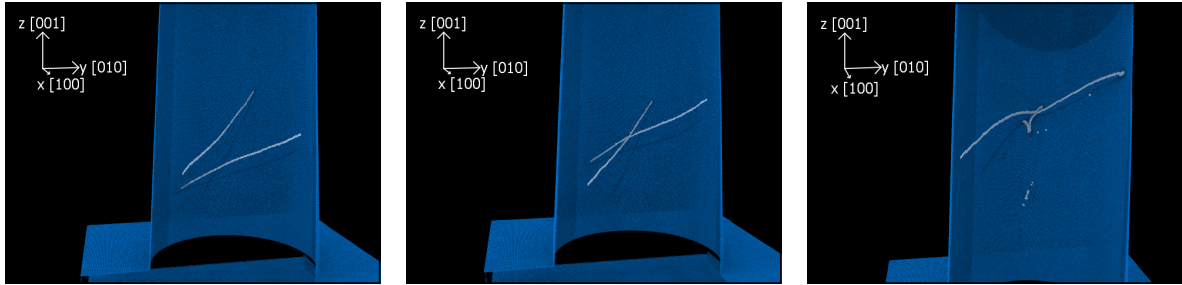

(a) The position of the dislocations at $\epsilon = 0$, after the relaxation.

(b) The dislocations have made contact and merged at $\epsilon = 0.0200$.

(c) The intersection between the two dislocations have moved along the dislocation lines toward the surface. One of the dislocations creates a loop at $\epsilon = 0.0425$.

Figure 8.14: The movement of the dislocations inside Pillar Model 1 during the simulation with temperature 300K and high strain rate.

(a) The position of the dislocations at $\epsilon = 0$, after the relaxation.

(b) The dislocations have made contact and merged at $\epsilon = 0.0059$.

(c) The two dislocations that previously merged, separates at $\epsilon = 0.0268$.

Figure 8.15: The movement of the dislocations inside Pillar Model 1 during the simulation with temperature 300K and low strain rate.
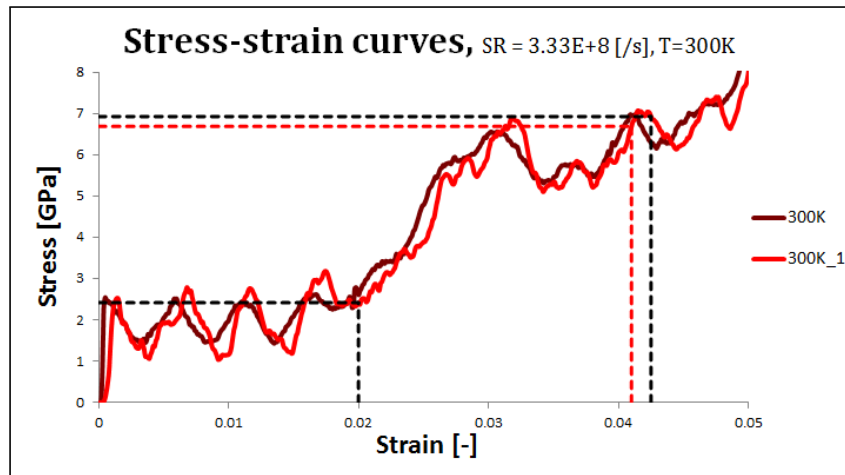

Figure 8.16: The stress strain curve of Model 1 and the pillar with no initial dislocations at high strain rate and room temperature. The red line indicates the point where the first dislocations appear from the base of the pillar. The black lines are the time steps of the simulation corresponding to the pictures in Figure 8.14.
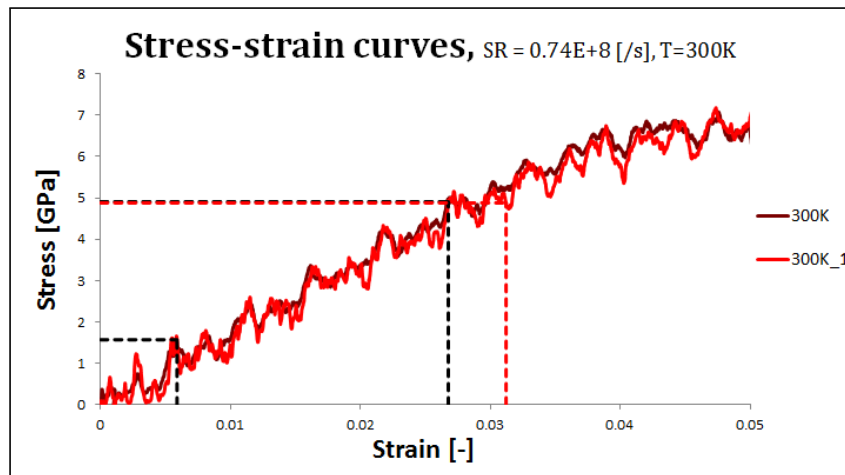
Figure 8.17: The stress strain curve of Model 1 and the pillar with no initial dislocations at low strain rate and room temperature. The red line indicates the point where the first dislocations appear from the base of the pillar. The black lines are the time steps of the simulation corresponding to the pictures in Figure 8.15.

8.3.2   300K - Model 2

For the simulations of Model 2 at the temperature 300K and high strain rate, the dislocations have merged during the relaxation of the system. The two dislocations move upward in the pillar in a similar manner as for the Pillar Model 1 at low strain rate and high temperature. The two dislocation lines does not become so horizontal though, and at 0.0350 strain they separate. This is illustrated in Figure 8.18 and Figure 8.21. The dislocations do not move as quickly after they separate, and still remain close together in the pillar at the point of yield.

   For the same model simulated at low strain rate, the two dislocations move a long distance up in the pillar and leave behind a large amount of debris before separating at 0.0197 strain, see Figure 8.19. The dislocation positioned to the right side of the pillar in Figure 8.19c leave the pillar as the simulation continues, but the dislocation to the left start to form a loop as illustrated in Figure 8.20. The loop increases in size and creates two new dislocations which moves in opposite directions. It can be seen in Figure 8.22 though, that this happen very close to the same time as new dislocations are created at the base of the pillar.
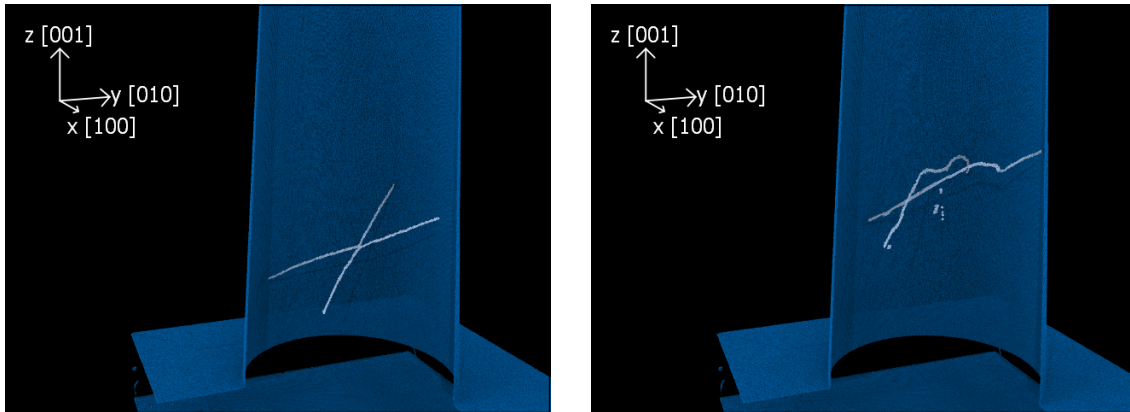
(a) The position of the dislocations at $\epsilon = 0$, after the relaxation.

(b) The dislocations separate at $\epsilon = 0.0350$.

Figure 8.18: The movement of the dislocations inside Pillar Model 2 during the simulation with temperature 300K and high strain rate.
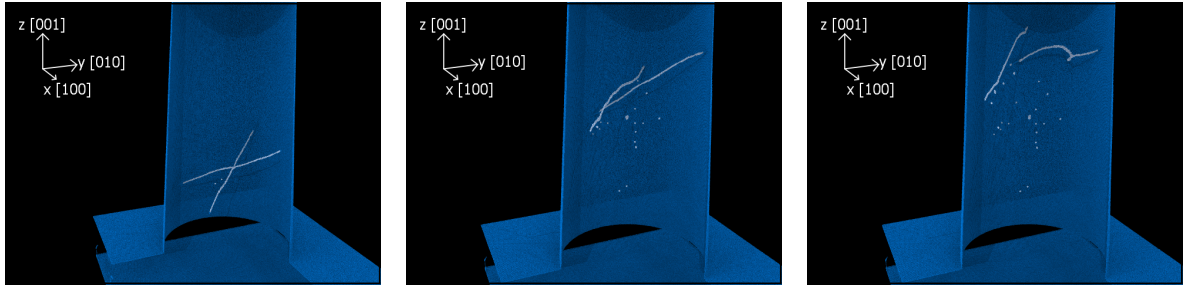
(a) The position of the dislocations at $\epsilon = 0$, after the relaxation.

(b) The dislocations separate at $\epsilon = 0.0197$.

(c) The picture is taken at $\epsilon = 0.0241$, shortly before one of the dislocations leave the pillar.

Figure 8.19: The movement of the dislocations inside Pillar Model 2 during the simulation with temperature 300K and low strain rate. The dislocations leave behind a lot of debris in their path.
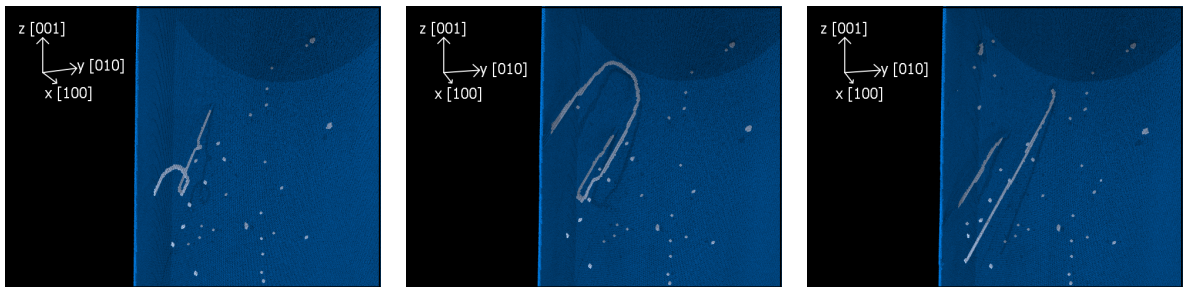
(a) The loop is created at $\epsilon = 0.0330$.

(b) The picture is taken at $\epsilon = 0.0354$ as the loop increases in size.

(c) Two new screw dislocations are created at $\epsilon = 0.0372$.

Figure 8.20: Dislocation movement observed for Pillar Model 2 at high temperature and low strain rate. The remaining dislocation forms a loop, much like the one in Figure 8.14c. This loop however starts some time before new dislocations are created at the base of the pillar, and increases in size until it connects with the surface and create two new screw dislocations.
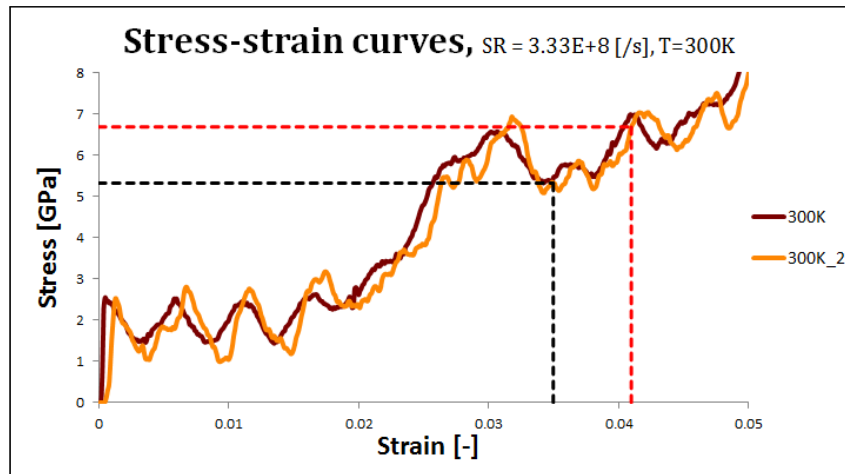
Figure 8.21: The stress strain curve of Model 2 and the pillar with no initial dislocations at high strain rate and room temperature. The red line indicates the point where the first dislocations appear from the base of the pillar. The black line is the time steps of the simulation corresponding to the picture in Figure 8.18b.
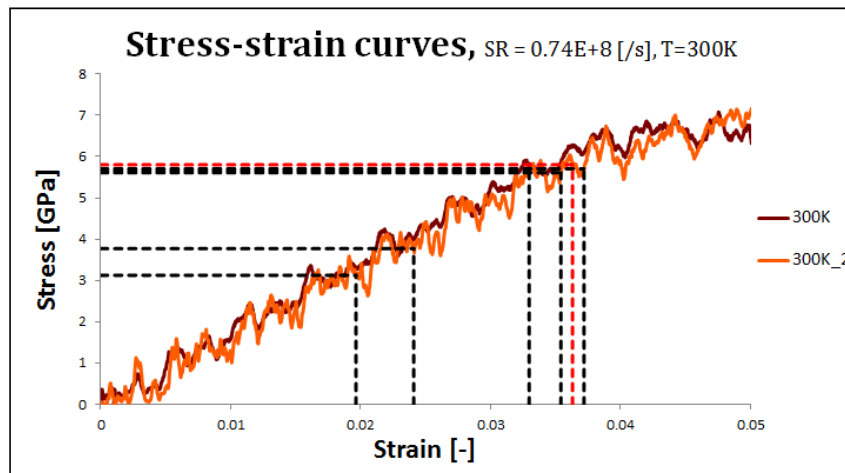

Figure 8.22: The stress strain curve of Model 2 and the pillar with no initial dislocations at low strain rate and room temperature. The red line indicates the point where the first dislocations appear from the base of the pillar. The black lines are the time steps of the simulation corresponding to the pictures in Figures 8.19 and 8.20.

8.3.3 300K - Model 3

The simulation for Model 3 at high temperatures and low strain rate is illustrated in Figure 8.23. The two dislocations which are very much the same as the ones inserted in Model 1, start to move toward each other immediately and merge at 0.0055 strain. The two dislocations initially keep moving in the same direction, causing the intersection between them to move toward the surface of the pillar. As the intersection reaches the surface at 0.0192 strain, the dislocations separate and disappears into the surface themselves after a short period of time. The dislocation positioned highest up in the pillar at the beginning of the simulation start moving at the same time as the two dislocations previously mentioned. It moves slowly and steadily some distance upwards in the pillar until the approximate time of the picture in Figure 8.23d, at which point it forms a loop and leaves through the surface at the top of the pillar at relatively high speed. Interestingly, it can be seen from Figure 8.24 that all these three dislocations mentioned leave the pillar a relatively long time before the stress is high enough for the new dislocations to emerge from the pillar base. This leaves only the two dislocations positioned at the base of the pillar which barely moves at all, even after yield has occurred.
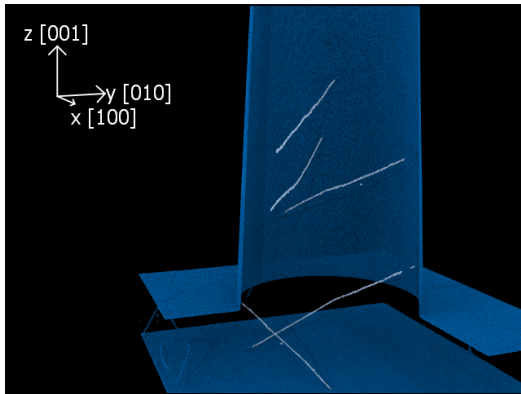
(a) The position of the dislocations at $\epsilon = 0$, after the relaxation.
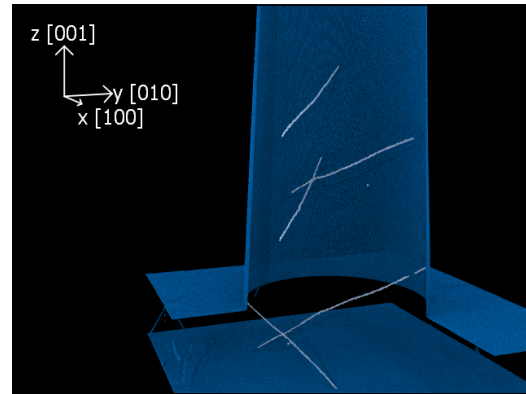
(b) Two of the dislocations make contact and merge at $\epsilon = 0.0055$.
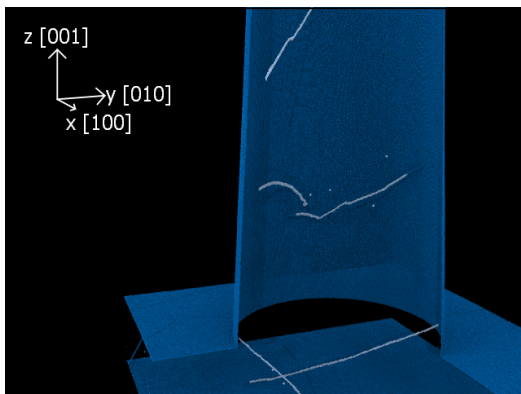
(c) The two dislocations that previously merged, separates at $\epsilon = 0.0192$.
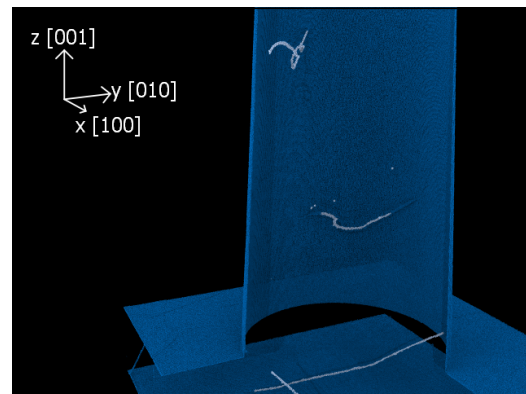
(d) At $\epsilon = 0.0226$, one of the dislocations have already left the pillar while two of the others are about to leave as well.

Figure 8.23: The movement of the dislocations inside Pillar Model 3 during the simulation with temperature 300K and low strain rate. The three dislocations at the top of the pillar disappears completely before any new dislocations are created at the base of the pillar.

Figure 8.24: The stress strain curve of Model 3 and the pillar with no initial dislocations at low strain rate and room temperature. The red line indicates the point where the first dislo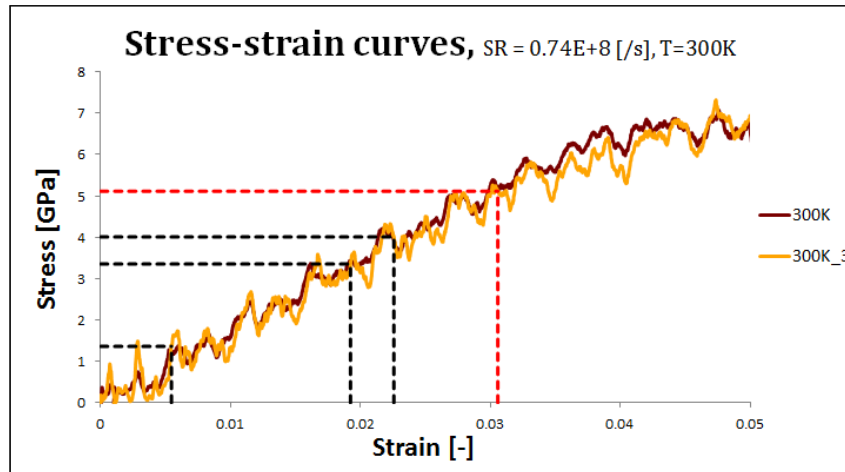cations appear from the base of the pillar. The black lines are the time steps of the simulation corresponding to the pictures in Figure 8.23.

9 | Pillar fabrication

In total, 15 pillars were successfully machined in the grain with the orientation <149>, while 16 pillars were successfully machined in the grain with orientation <235>. The dimensions of the pillars created are listed in Tables 9.1 and 9.2. Pictures of all the pillars were also taken shortly after fabrication but prior to the compression testing. Some of the pillars were discarded as their dimensions or geometry did not satisfy the quality required for good results from the compression testing. Pictures of the pillars that were deemed good enough for further testing are included in Figures 9.1 and 9.2.

Orientation <149>	Height [µm]	Diameter, top [µm]
Pillar: 6	3.0	1.0
Pillar: 15	3.4	1.0
Pillar: 4, 9, 12	3.5	1.0
Pillar: 1, 3, 5, 13, 14	3.6	1.0
Pillar: 8, 10, 11	3.7	1.0
Pillar: 7	3.8	1.0
Pillar 2	3.9	1.0

Table 9.1: The dimensions of the pillars created in the <149>-direction.

Orientation <235>	Height [µm]	Diameter, top [µm]
Pillar: 3	2.8	1.0
pillar: 2	3.0	1.0
Pillar: -2	3.3	1.0
Pillar: 6	3.4	0.9
Pillar: 13, 14	3.4	1.0
Pillar: 11	3.5	0.7
Pillar: 7, 8, 9, 10, 15	3.5	1.0
Pillar: -1	3.8	1.0

Table 9.2: The dimensions of the pillars created in the <235>-direction.
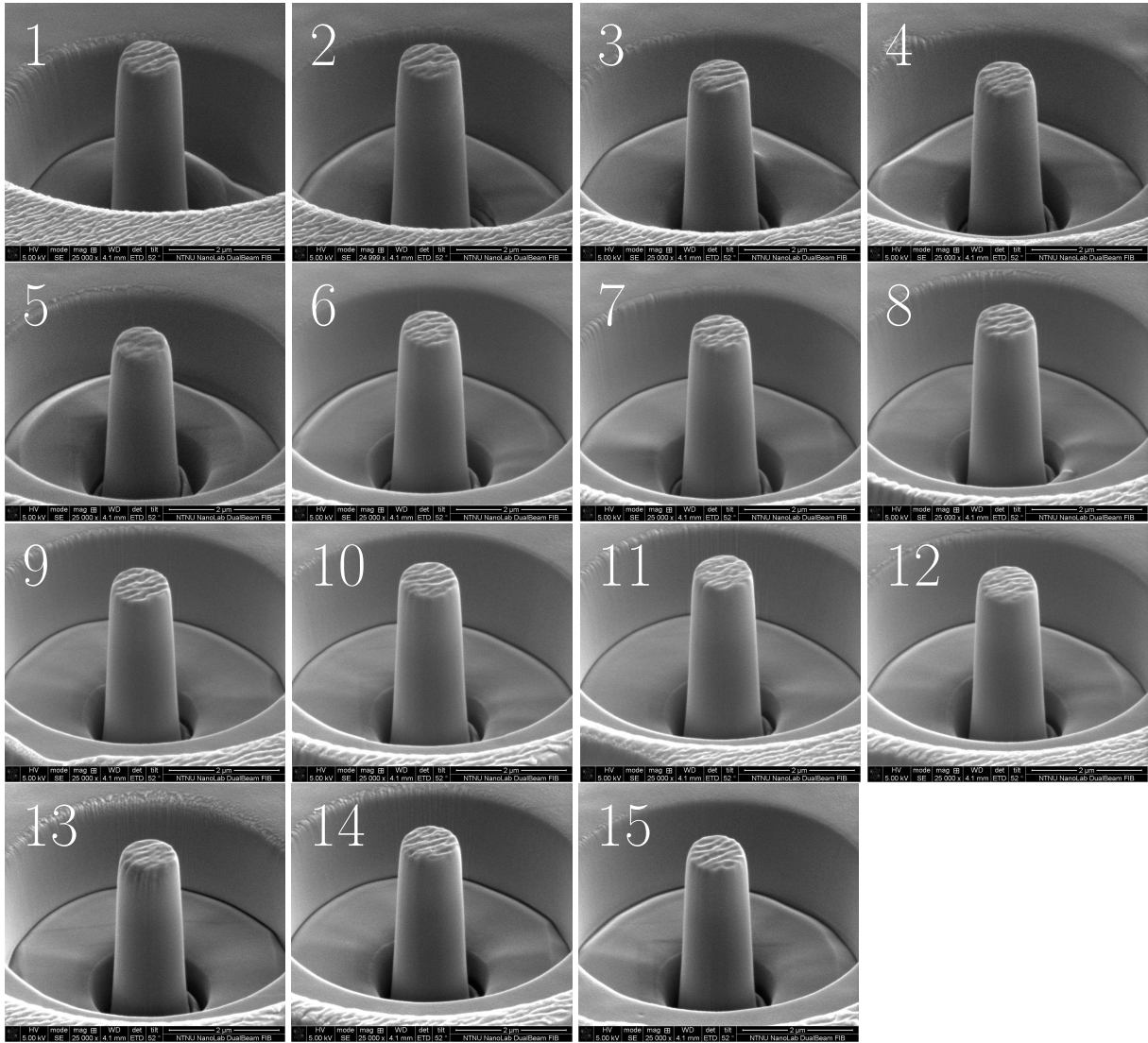
Figure 9.1: Pictures of all the pillars created in the grain with <149>-orientation. The pictures was taken right after fabrication, prior to the compression testing.
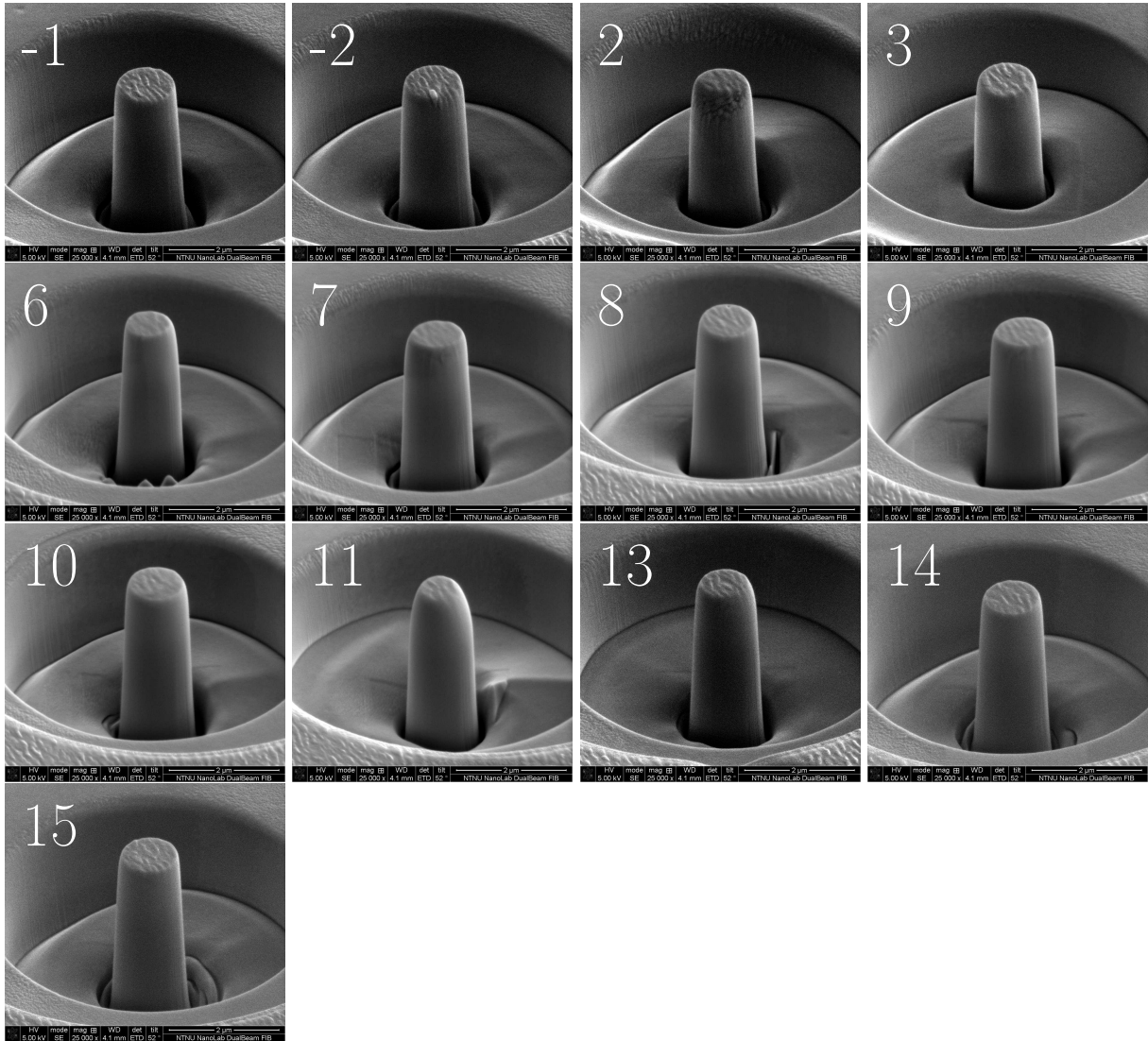
Figure 9.2: Pictures of all the pillars created in the grain with <235>-orientation. The pictures was taken right after fabrication, prior to the compression testing.

10 | Indentation of micropillars

The micropillars were indented at two temperatures; room temperature and -80°C. The following sections show pictures of the pillars after compression and the resulting stress-strain curves acquired. No extensive analysis of the results from the experimental testing were performed as the results were acquired very late in the process of writing this thesis. The results are therefore presented mostly as a documentation of the work performed, and will be analysed for use in later reports by PhD Anette B. Hagen.

10.1 <149>-orientation, room temperature

7 pillars in the <149>-oriented grain were compressed at room temperature. The pictures of the pillars taken after the compression is illustrated in Figure 10.1 while the resulting stress strain curves are illustrated in Figure 10.2.

Figure 10.1: Pictures of the pillars in the grain with <149>-orientation, taken after indentation at room temperature.

Figure 10.2: The stress strain curves acquired from the pillars with <149> orientation, indented at room temperature.

10.2 <149>-orientation, -80°C

8 pillars in the <149>-oriented grain were compressed at -80°C. The pictures of the pillars taken after the compression is illustrated in Figure 10.3 while the resulting stress strain curves are illustrated in Figure 10.4.

Figure 10.3: Pictures of the pillars in the grain with <149>-orientation, taken after indentation at a temperature of −80°C.

Figure 10.4: The stress strain curves acquired from the pillars with <149> orientation, indented at -80°C.

10.3 <235>-orientation, room temperature

6 pillars in the <235>-oriented grain were compressed at room temperature. The pictures of the pillars taken after the compression is illustrated in Figure 10.5 while the resulting stress strain curves are illustrated in Figure 10.6.

Figure 10.5: Pictures of the pillars in the grain with <235>-orientation, taken after indentation at room temperature.

Figure 10.6: The stress strain curves acquired from the pillars with <235> orientation, indented at room temperature.

10.4 <235>-orientation, -80°C

7 pillars in the <235>-oriented grain were compressed at -80°C. The pictures of the pillars taken after the compression is illustrated in Figure 10.7 while the resulting stress strain curves are illustrated in Figure 10.8.
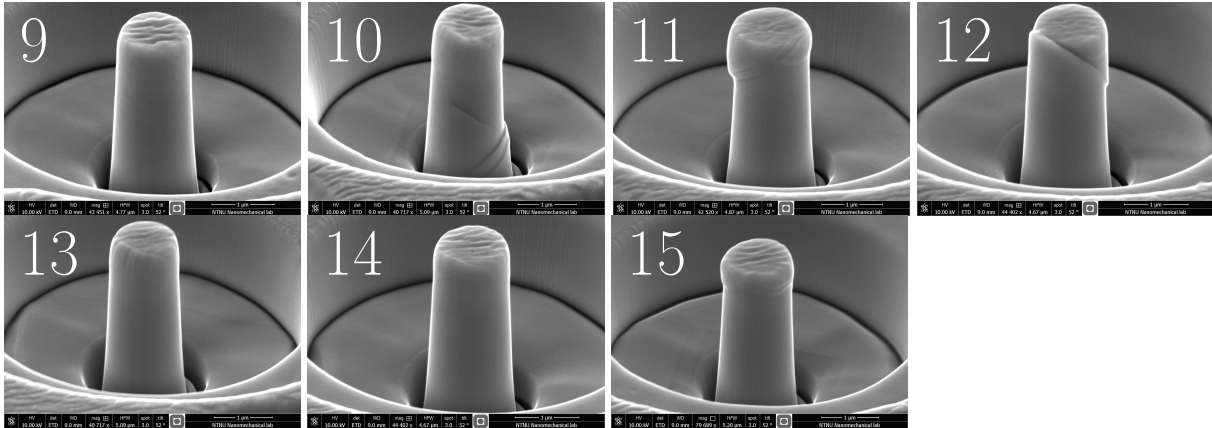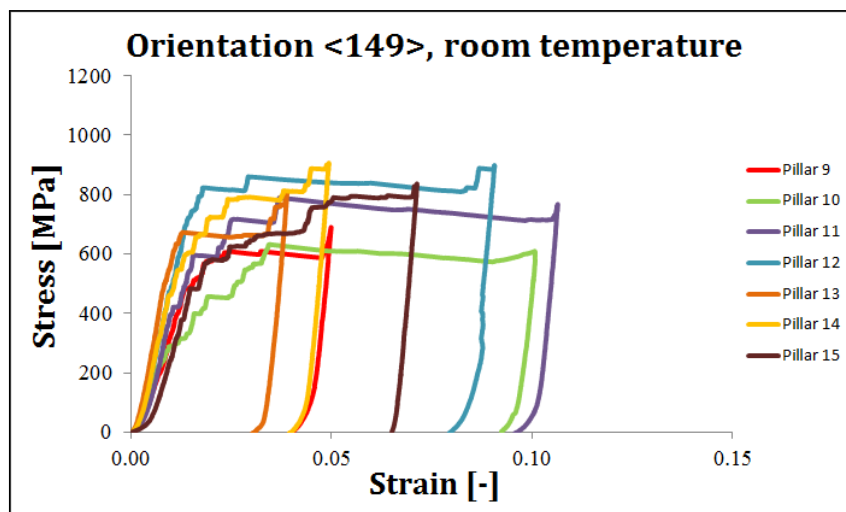

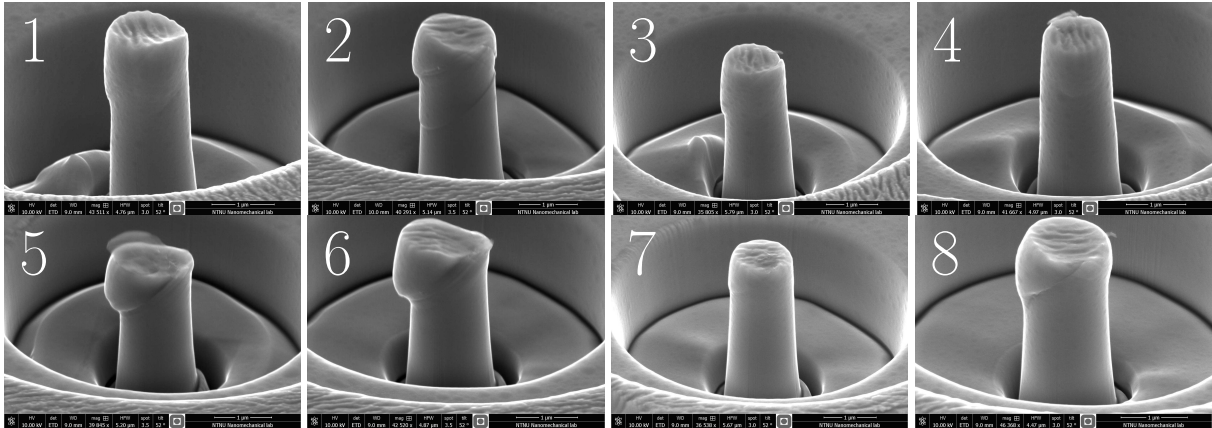**Figure 10.7:** Pictures of the pillars in the grain with <235>-orientation, taken after indentation at a temperature of −80°C.
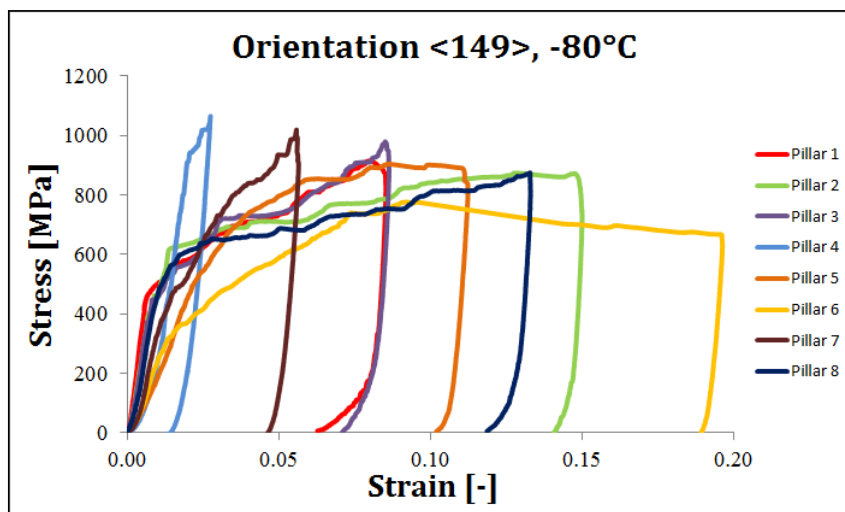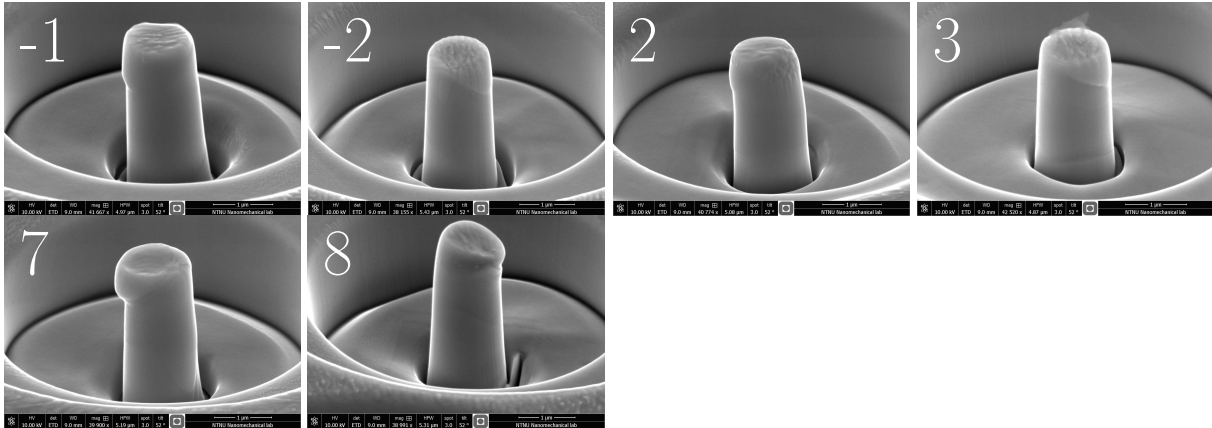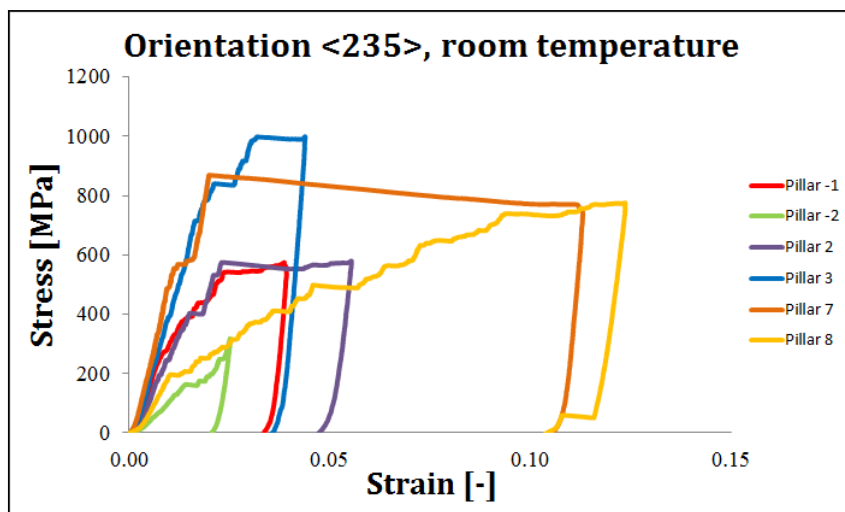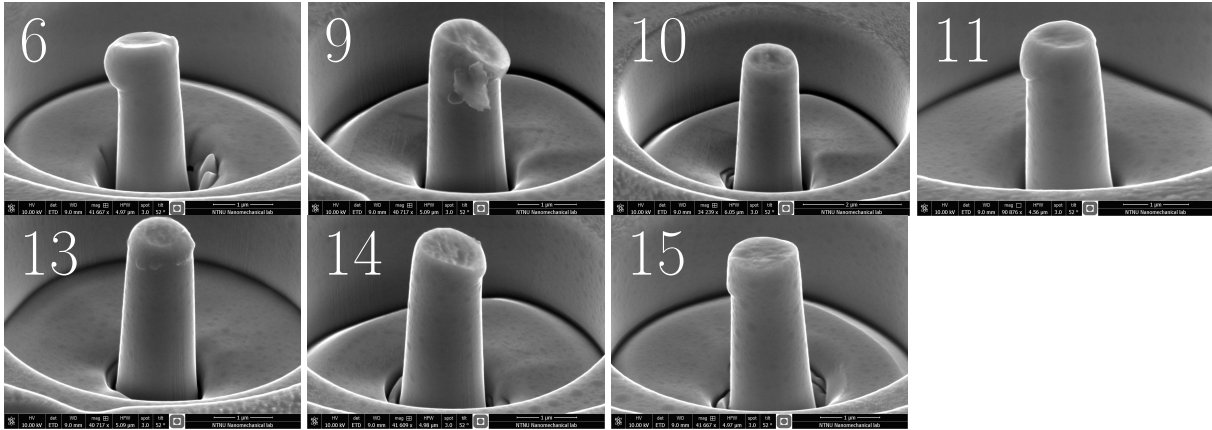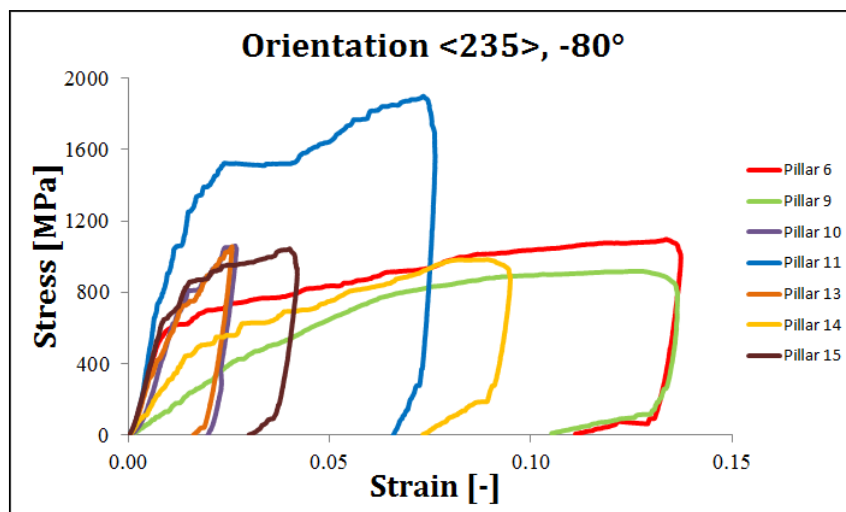

Figure 10.8: The stress strain curves acquired from the pillars with <235> orientation, indented at -80°C.

11 | Discussion

Creating and running the simulations

For this thesis, three different simulation models of pillars with initial dislocation were successfully developed, in addition to a model with no initial dislocations. The size limitations previously experienced with the use of the program Atomsk was overcome, and the pillars were created with a diameter of 500Å. The increase in size is believed to have contributed to better and more accurate simulation results. For instance, the initial pillar geometry was not visibly affected by the insertion of dislocations as the volume of the pillar in comparison to the dislocations was increased, reducing the overall influence of this source of error. Ideally, the pillar diameter should be increased even more to get closer to the diameters of the pillars used in experimental testing, but even at this size the simulations became very time consuming and required large amounts of space for computer data storage. The size of the dump-files were also occasionally a problem for the visualisation program Ovito. Last but not least, the development of the three simulation models took a lot of time as large amounts of data had to be converted between LAMMPS and Atomsk, and then visualised in Ovito to check whether or not the insertion of the dislocations were successful. The process had to be repeated each time a change was to be made to the model, or if an error occured with the positioning of the dislocations. Atomsk is still evaluated to be a program suitable for the task of inserting dislocations into nanopillars, but some small issues regarding unwanted lattice changes at certain combinations of dislocation positions should be investigated before extensive use of the program for insertion of multiple dislocations. It is not clear though whether the issue is in the commands issued to the program or in the program itself.

The simulation script used to simulate the compression of the nanopillars was adapted from the script that was used in the project work leading up to the thesis. A few changes was made in regard to the pillar model itself, and a new section was added in order to increase the velocity of the indenter gradually up to the constant value for the displacement controlled indenting, rather than making the indenter collide with the pillar at full speed. The code section should be changed before further use as it was not altogether correctly written, but more accurate results were achieved by the use of it.

Strain rate

Strain rate was originally not a variable to be examined in the work with this thesis, but as the stress-strain curves achieved from the first simulation results were inaccurate and not very satisfactory it was decided to lower the strain rate and re-run the simulations in order to get better results. An investigation of the strain rate dependency on the pillar simulations was also recommended by several people, including my supervisor, in order to see how the strain rate affected the dislocations inserted into the pillars. It was discovered that the a change in strain rate affected the fluctuations of the stress strain curve and the yield stress of the simulations a lot. A report on similar pillar compression simulations recommended that the strain rate should not be exceed $5 \cdot 10^8 s^{-1}$ in order to avoid inaccurate results due to a high strain rate [15]. Based on the results in this thesis, a strain rate higher than approximately $1 \cdot 10^8 s^{-1}$ should be avoided.

The simulations with different strain rates showed that as the strain rate was decreased, the yield stress of the simulations decreased as well. This was as expected. What was not expected was how well the points for the yield stresses corresponded to each other as they were compared in the same plot, based on the strain rate used to achieve them. The yield stresses showed a very clear trend, which very possibly can be used to develop an equation describing the strain rate dependency of pillar strength. However the range of the strain rate values over which the yield points were measured is too small to determine the correlation with certainty, as small chances in the equation could lead to huge changes in the resulting stresses at strain rates which are orders of magnitude lower. In order to get a better basis for the development of such an equation, it would be recommended to run time consuming simulations at as low strain rates as possible, as well as investigating further into existing literature. It should be taken into consideration that such an equation would necessarily be very dependant on temperature, and possibly also specimen size.

Based on Figures 8.1 - 8.4, high strain rate was observed to cause a large drop in stress after yield. For the low strain rate, the drop was much smaller. As the high strain rate initially had a higher yield stress, the resulting stress value reached after the drop is surprisingly very similar for the two strain rates. This seem to be the case for both of the temperatures. If this is actually the case, it could indicate that the stress after yield is independent of strain rate. However this is very unlikely as the same effect was not observed for the stress-strain curves in Figure 7.1.

The modulus of elasticity was observed to be increasing as the strain rate was decreasing. At the highest strain rate, $3.33 \cdot 10^8 s^{-1}$ and for high temperature, the modulus was measured to be 152GPa, which is some distance away from the reference value of 211GPa for bulk iron. But as the modulus of elasticity increased to 172GPa for the simulation with the lowest strain rate at $0.44 \cdot 10^8 s^{-1}$, it is believed that the value would increase a lot for strain rates of the same magnitude as the ones used in experimental tests. The E modulus was also observed to have a larger value at low temperature, but the difference was in the order of just 2-3 GPa.

Simulations with initial dislocations

Overall, the insertion of dislocations into the pillars did not affect the results of the simulations in a major way. The stress-strain curves were very similar for both the models with and without initial dislocations. One difference that was observed however, was that the fluctuations for the stress-strain curves were higher for the simulated pillars with no initial dislocations. This was observed for the simulations in the previous project work as well. Therefore, the insertion of initial dislocations does lead to a more smooth curve. This is possible due to the ability of the dislocations to move inside the pillar in order to release energy, allowing the dislocations to dampen the stress fluctuations by moving.

The largest change in dislocation behaviour for the simulations performed for this thesis compared to the ones performed in the previous project work, was that all the dislocations stayed in the pillar after the relaxation of the system. None of the dislocations did leave the pillar immediately as the compression started, and most of them were actually still present in the pillar as the yield stress was reached. Previously it was observed that the dislocations very quickly left the pillars as the mirror forces working on the dislocations were much higher than the driving forces on the dislocations from the surface of the pillar. This change in dislocation behaviour is believed to be due to the much larger diameter of these new pillar simulations. The forces driving the dislocations toward the surface will be smaller as the diameter of the pillar increases, but the extent was surprising.

At low temperature, some of the dislocations barely moved along the pillar surface at all. None of the dislocations left the pillar prior to yield. The dislocation lines however, did create what appeared to be kinks and even kink-pairs travelling up and down the dislocation line. Apart from these kinks, the rest of the dislocation lines were very straight and smooth. The dislocations that did move inside the pillar, moved in the upwards direction (toward the force applied). The movement happened as the kinks reached the surface of the pillar and forced the end point of the dislocation line to move an equivalent distance. This corresponds well with the description of screw dislocation motion at low temperature as depicted in literature. At room temperature, the dislocations were much more mobile. The dislocation lines chose to move around with a more circular shape instead of the straight lines observed at low temperature. As the stress increased, the dislocations simulated at room temperature frequently formed small loops and circular shapes which travelled along the dislocation lines or developed into new shapes. These loops sometimes detached from the dislocation lines, forming large amounts of debris in the dislocation path. Sometimes the loops increased in size instead, and developed into new dislocations. However this always happened as the stress was close to yield.

For the simulations with room temperature, some of the dislocations left the pillars shortly before yield. The ones that left belonged to the simulations with low strain rate. The ones simulated at a high strain rate stayed in the pillar. A similar tendency was observed for the low temperature simulations where the dislocations connected in the simulation of Model 1 at low strain rate, stayed separate and did not seem to move position at all when simulated with the high strain rate. This would indicate that at a lower strain rate the stress is increased at a lower rate, allowing the dislocations to move more easily before high stresses are reached. This makes dislocation starvation more likely at even lower strain rates.

For the simulations of Model 3 it was observed that the two dislocations positioned

in/near the base of the pillar, did not move much at all. It is uncertain whether they had an effect on the simulation or if their position made them unaffected by the pillar compression. The other three dislocations seem to be slightly more mobile than the ones observed in Model 1 and 2. At high temperature, all three of the dislocations have left the pillar a relatively long time before the stress for which new dislocations emerge from the pillar base. For the low temperature case, all three of the top dislocations stays in the pillar until yield is reached. However, two of the dislocations both connects *and* separate prior to the initiation of new dislocations from the base. None of the other dislocations simulated at low temperature have had enough energy to separate before yield once connected. Based on these observations it would seem like the dislocations are more mobile when there are a higher number of dislocations in close proximity.

Experimental testing

Unfortunately, there was no time for extensive analysis of the results acquired from the experimental testing as there was experienced problems with the equipment used. However it could be seen from the experimental results as well that the yield strength measured increased for lower temperatures and that the different orientations showed different properties. For some of the pillars, activated slip planes were clearly visible while other pillars were more evenly compressed. All taken into consideration, including experimental testing to the master's thesis is considered a success as it contributed greatly to the overall understanding of the whole process.

12 | Conclusion

In this thesis, three models of a nanopillar with initial dislocations have been successfully created. It is concluded that the insertion of initial dislocations into nano sized pillars under the conditions specified, do reduce the fluctuations of the stress-strain curves and probably makes for a more realistic model of the simulated system. However, the dislocations have not affected the yield stress or the general shape of the stress-strain curve in a significant way. A change in the number of dislocations or their positions in the pillar does not seem to have any effect on the resulting stress-strain curve.

The yield stress of the simulated iron nanopillar is concluded to be highly dependent on the simulation strain rate. As is the accuracy of the received stress-strain curves which show high fluctuations at high strain rates. A strain rate above an approximate value of $1 \cdot 10^8 s^{-1}$ is therefore not recommended for atomistic simulations of pillar compression.

The dislocations inserted in the pillars were observed to be more mobile at high temperatures and low strain rate. At low temperature the dislocations were observed to move mainly by the creation of kinks, if they did move at all. The dislocations did not try to leave the pillar immediately after the start of the simulation as previously experienced. Most of the dislocations were present in the pillar at the point of yield.

References

[1] Olaisen M. *Atomistic modelling of deformation and fracture – Arctic materials* [project work]. Trondheim: NTNU; 2014.

[2] Sandia National Laboratories. *LAMMPS Molecular Dynamics Simulator* [Internet]. 2004 [cited 2015 June 1]. Available from: http://lammps.sandia.gov/

[3] *About Vilje.* Available from: https://www.hpc.ntnu.no/display/hpc/About+Vilje

[4] Hirel P. *Atomsk* [Internet]. 2010 [Cited 2015 June 1]. Available from: http://pierrehirel.info/codes_atomsk.php?lang=eng

[5] Stukowski A. *Visualization and analysis of atomistic simulation data with OVITO – the Open Visualization Tool* [Internet]. 2010 [Cited 2015 June 1]. Available from: http://www.ovito.org/

[6] Sintef. *Arctic Materials* [Internet]. 2010 [cited 2015 June 1]. Available from: http://www.sintef.no/Projectweb/Arctic-Materials/

[7] Buehler MJ. *Atomistic Modeling of Materials Failure.* Cambridge: Springer; 2008

[8] Dieter GE. *Mechanical Metallurgy.* SI Metric Edition. UK: McGraw-Hill Book Company; 1988

[9] Hull D, Bacon DJ. *Introduction to Dislocations.* 5th ed. UK: Elsevier; 2011

[10] Available from: http://poh101.com/index3/mems.html

[11] Frenkel, J. *Zur Theorie der Elastizitätsgrenze und der Festigkeit kristallinischer Körper.* Zeitschrift für Physik, 1926. 37(7-8):572-609.

[12] Schmid E, Boas W. *Kristallplastizität: Mit Besonderer Berücksichtigung der Metalle.* Springer; 1935

[13] Rogne BRS, Thaulow C. *Strengthening mechanisms of iron micropillars.* Philosophical Magazine. 2014 DOI:10.1080/14786435.2014.984004

[14] Jennings AT, Li J, Greer JR. *Emergence of strain-rate sensitivity in Cu nanopillars: Transition from dislocation multiplication to dislocation nucleation.* Acta Materialia. 2011;59(14):p5627-5637 DOI:10.1016/j.actamat.2011.05.038

[15] Ersland CH, Thaulow C. *Modeling of size and strain rate effects in compression tests of iron nanopillars.* 2012

[16] Naamane S, Monnet G, Devincre B. *Low temperature deformation in iron studied with dislocation dynamics simulations.* International Journal of Plasticity. 2009;26(1):84-92. DOI:10.1016/j.ijplas.2009.05.003

[17] Caillard D. *Kinetics of dislocations in pure Fe. Part II. In situ straining experiments at low temperature.* Acta Materialia. 2010;58(9):3504-3515. DOI:10.1016/j.actamat.2010.02.024

[18] Available from: http://www.tankonyvtar.hu/en/tartalom/tamop425/0036_Dislocations_EN/jogs-_and_kinks.html

[19] Vatne, IR. *Quasicontinuum modeling of fracture in bcc materials* [Doctoral thesis]. Trondheim: NTNU; 2012

[20] Greer JR, Nix WD. *Nanoscale gold pillars strengthened through dislocation starvation.* Physical Review B. 2006;73(24):245410. DOI: 10.1103/PhysRevB.73.245410

[21] Weinberger CR, Cai W. *Surface-controlled dislocation multiplication in metal micropillars.* 2008;105(38):14304–14307.

[22] Lowry MB, et al. *Achieving the ideal strength in annealed molybdenum nanopillars.* Acta Materialia. 2010;58(15):p5160-5167. DOI: 10.1016/j.actamat.2010.05.052

[23] Available from: http://www.norfab.no/technologies/characterization/ntnu-nanolab/fib/

[24] Uchic MD, Dimiduk DM, Florando JN, Nix WD. *Exploring specimen size effects in plastic deformation of Ni3(Al,Ta).* MRS Proceedings. 2002. DOI:10.1557/PROC-753-BB1.4

[25] Mendelev MI, Han S, Srolovitz DJ, Ackland GJ, Sun DY, Asta M. *Development of new interatomic potentials appropriate for crystalline and liquid iron.* Phil. Mag. Taylor and Francis; 2003

[26] Hagen AB. *In-situ Compression Testing of Nanosized Pillars* [master's thesis]. Trondheim: NTNU; 2014.

[27] Greina K. *In-situ fracture mechanical testing of microsized cantilevers* [master's thesis]. Trondheim: NTNU; 2014.

Appendix

A | Appendix - LAMMPS code

An example of the simulation code for the pillar with a temperature of 300K simulated with the low strain rate.

```
##### CREATING THE BOX #####

variable          filename string d500_300_0.74K

package           omp 4
processors        4 4 *
dimension         3
boundary          p p p
units             metal

read_data         500_300dd.lmp              ## If atomsk is used


##### VARIABLES #####

# Variables for the pillar
variable          latlength equal 2.85896    #Length for 300K
#variable         xfactor equal 1.39104       #235
#variable         yfactor equal 1.37199       #235
#variable         zfactor equal 1.62221       #235
#variable         xlength equal sqrt(323)     #235
#variable         ylength equal sqrt(34)      #235
#variable         xfactor equal 1.104315      #149
#variable         yfactor equal 1.36094       #149
#variable         zfactor equal sqrt(2)       #149
#variable         xlength equal sqrt(82)      #149
#variable         ylength equal sqrt(2009)    #149
variable          xfactor equal 1             #001
variable          yfactor equal 1             #001
variable          zfactor equal 1             #001
variable          xlength equal 1             #001
variable          ylength equal 1             #001

variable   size equal 1510
#variable  d_x equal round(${size}/${latlength}/${xfactor}*0.75)

#variable  d_y equal round(${size}/${latlength}/${yfactor}*0.75)
#variable  d_z equal round(${size}/${latlength}/${zfactor})


#lattice          bcc ${latlength} orient x 17 -3 -5 orient y 0 5 -3
                  orient z 2 3 5
#lattice          bcc ${latlength} orient x 9 0 -1 orient y -2 41 -18
                  orient z 1 4 9
#lattice          bcc ${latlength} orient x 1 0 0 orient y 0 1 0 orient
                  z 0 0 1

#region           box block 0 ${d_x} 0 ${d_y} 0 ${d_z}
#create_box       1 box
#create_atoms     1 box
```

```
##### FORCE FIELD, POTENTIAL #####

mass        * 55.845                # Atom mass, iron
pair_style eam/fs/omp
pair_coeff * * Fe_2.eam.fs Fe



##### VARIABLES #####

variable   d equal 500             # Diameter of pillar
variable   r equal $d/2            # radius of pillar
variable   h equal round($d*2.5)   # Height of pillar
variable   hb equal round($d/2)    # height of the base
variable   htot equal (${hb}+$h)
           # height of the base and cylinder
variable   lengthxy equal xhi
           # length of system in x- and y-direction
variable   center equal round(${lengthxy}/2)
           # x- and y-coordinates of the center of the base
variable   zl equal zlo
variable   radl equal $r+(0.0524*$h)
variable   ycutmin equal ${center}-(floor($d*3*0.75/${ylength}
           /${latlength})*${ylength}*${latlength}/2)
variable   ycutmax equal ${center}+(floor($d*3*0.75/${ylength}
           /${latlength})*${ylength}*${latlength}/2)
variable   xcutmin equal ${center}-(floor($d*3*0.75/${xlength}
           /${latlength})*${xlength}*${latlength}/2)
variable   xcutmax equal ${center}+(floor($d*3*0.75/${xlength}
           /${latlength})*${xlength}*${latlength}/2)



# Timestep and temperature
variable   temp equal 300
variable   ts equal 0.0015
timestep   ${ts}
variable   nrun equal 900000     # Number of time steps in main run
variable   nrelax equal 50000    # Number of time steps in relaxation
variable   nrampsteps equal 20000    # Number of time steps in ramp
variable   ramped equal ${nrelax}+${nrampsteps}

# Variables for strain and velocity
variable   maxstrain equal 0.1
           # the system should run to a strain of 15%
variable   vel equal -${maxstrain}*${htot}/${ts}/${nrun}
           # calculate indenter velocity
print      "indenter velocity = ${vel}"
```

```
##### Delete atoms #####

region          base block ${xcutmin} ${xcutmax} ${ycutmin}
                ${ycutmax} INF ${hb} units box  # Box of bottom atoms
region          cyl cone z ${center} ${center} ${radl} $r ${hb}
                ${htot} units box    # Cylinder

group     base region base     # defines the base into a group
group     cyl region cyl       # defines the pillar into a group
group     rest subtract all cyl base
          # defines all atoms except the base and pillar into a group

delete_atoms    group rest     # delete all atoms in "rest"
change_box      all z final 0 ${htot} units box
change_box      all x final ${xcutmin} ${xcutmax} units box
change_box      all y final ${ycutmin} ${ycutmax} units box

change_box      all boundary p p s


fix balance all balance 100000 1.05 shift xyz 50 1.05

region    bottomat block INF INF INF INF INF 1.25 units box
group     bottomat region bottomat
group     mobile subtract all bottomat


##### Computing #####
compute   pot all pe/atom
          # Computes potential energy per atom
compute   stress all stress/atom NULL
          # Computes virial stress per atom
variable  mises atom "0.707106781 * sqrt( (c_stress[1] -
          c_stress[2])^2 + (c_stress[2] - c_stress[3])^2 +
          (c_stress[1] - c_stress[3])^2 + 6*(c_stress[4]^2 +
          c_stress[5]^2 + c_stress[6]^2))"
          # Computes the von Mises stress for each atom

compute   cna all cna/atom 3.46
compute   current all reduce sum c_cna
thermo_style    custom step temp c_current
change_box      all z final 0 ${htot} units box # units lattice ${zl}

run 0 start 0 stop 0
variable        cnaatom atom "c_cna == 3"
group           bcc variable cnaatom

compute   myTemp mobile temp
compute   zmax all reduce max z
          # compute the highest z-coordinate
compute   zmin all reduce min z
          # compute the lowest z-coordinate
```

```
###### Dump and thermo ######

thermo          200
thermo_style    custom step temp press pxx pyy pzz c_zmax cpu
dump            5 all custom 5000 dump.relax_${filename}*.gz id type
                xs ys zs c_cna
dump_modify     5 thresh c_cna != 3


###### Running the relaxation ######

delete_atoms    overlap 1.0 all all
variable        zl equal zlo
minimize        1.0e-6 1.0e-8 1000 100000
velocity        all create ${temp} 731201

reset_timestep  0

# Relaxation
fix       1 mobile npt temp ${temp} ${temp} 0.1 drag 2.0 x 0.0 0.0
          1.5 y 0.0 0.0 1.5 drag 2.0 couple none
fix       indenter2 all indent 50.0 plane z ${zl} lo units box
          #alternative to setforce



run       ${nrelax}        # relaxation

undump    5

dump      all all custom 10000 dump.${filename}*.gz id type xs ys zs
          c_pot v_mises c_cna
dump      4 all custom 2000 dump.alpha_${filename}*.gz id type xs ys
          zs c_pot v_mises c_cna
dump      3 bcc custom 1000 dump.beta_${filename}*.gz id type xs ys
          zs c_pot v_mises c_cna     #Adds a second dump

dump_modify     4 thresh c_cna != 3
dump_modify     3 thresh c_cna != 3



##### Simulation #####

variable        zarelax equal c_zmax
                # current hight of pillar after relaxation
#variable       zpos equal ${zarelax}+${vel}*(step-
                ${nrelax})*dt*(step<=(${nrelax}+${nrun}))
variable        zpos equal ${zarelax}+((ramp(0,${vel}/2))*(step-
                ${nrelax})*dt)
#print          "zarelax = ${zarelax}, zpos = ${zpos}"
```

```
unfix          1
fix            1 mobile nvt temp ${temp} ${temp} 0.1 drag 2.0
               # Only control temperature during indentation, using
               an NVT fix
fix_modify     1 temp myTemp

fix            2 bottomat setforce 0.0 0.0 0.0
               # Keep the bottom layer of atoms fixed

fix            indenter all indent 50.0 plane z v_zpos hi units box
fix_modify     indenter energy yes
fix            aveindent all ave/time 20 10 200 f_indenter[3]
               # Perform averaging of the indenter force

log            log.${filename}
thermo_style   custom step temp f_indenter[3] v_zpos f_aveindent
               c_zmax cpu
thermo_modify  flush yes temp myTemp

run            ${nrampsteps} start ${nrelax} stop ${ramped}
variable       zpos delete
variable       postramp equal c_zmax
variable       zpos equal ${postramp}+${vel}*(step-${ramped})*dt

run            ${nrun}                        # running simulation
```

B | Appendix - Codes used in Atomsk

Code used to insert two dislocations inside a pillar.

300K:

```
atomsk dump.orient_500_300v3
-orient[100][010][001][101][12-1][-111]
-dislocation 0.48*BOX 0.48*BOX screw z x 2.4759 0.26
-orient[101][12-1][-111][-101][1-21][111]
-dislocation 0.44*BOX 0.46*BOX screw z x 2.4759 0.26
-orient[-101][1-21][111][100][010][001] -alignx 500_300dd.lmp
```

15K:

```
atomsk dump.orient_500_15
-orient[100][010][001][101][12-1][-111]
-dislocation 0.48*BOX 0.48*BOX screw z x 2.4727 0.26
-orient[101][12-1][-111][-101][1-21][111]
-dislocation 0.44*BOX 0.46*BOX screw z x 2.4727 0.26
-orient[-101][1-21][111][100][010][001] -alignx 500_15dd.lmp
```

Code used to insert two dislocations close together inside a pillar.

300K:

```
atomsk dump.orient_500_300v3
-orient[100][010][001][101][12-1][-111]
-dislocation 0.47*BOX 0.53*BOX screw z x 2.4759 0.26
-orient[101] [12-1][-111][-101][1-21][111]
-dislocation 0.44*BOX 0.48*BOX screw z x 2.4759 0.26
-orient[-101][1-21][111][100][010][001] -alignx 500_300df.lmp
```

```
atomsk dump.orient_500_15
-orient[100][010][001][101][12-1][-111]
-dislocation 0.47*BOX 0.53*BOX screw z x 2.4727 0.26
-orient[101] [12-1][-111][-101][1-21][111]
-dislocation 0.44*BOX 0.48*BOX screw z x 2.4727 0.26
-orient[-101] [1-21][111][100][010][001]
-alignx 500_15df.lmp
```

Code used to insert five dislocations inside a pillar.

300K:
```
atomsk dump.orient_500_300v3
-orient[100][010][001][101][12-1][-111]
-dislocation 0.44*BOX 0.47*BOX screw z x 2.4759 0.26
-dislocation 0.503*BOX 0.457*BOX screw z x 2.4759 0.26
-orient[101][12-1][-111][-101][1-21][111]
-dislocation 0.467*BOX 0.423*BOX screw z x 2.4759 0.26
-dislocation 0.31*BOX 0.39*BOX screw z x 2.4759 0.26
-orient[-101][1-21][111][1-2-1][101][-1-11]
-dislocation 0.4*BOX 0.27*BOX screw z x 2.4759 0.26
-orient[1-2-1][101][-1-11][100][010][001]
-alignx 500_300yes.lmp
```

15K:
```
atomsk dump.orient_500_15
-orient[100][010][001][101][12-1][-111]
-dislocation 0.44*BOX 0.47*BOX screw z x 2.4727 0.26
-dislocation 0.503*BOX 0.457*BOX screw z x 2.4727 0.26
-orient[101][12-1][-111][-101][1-21][111]
-dislocation 0.467*BOX 0.423*BOX screw z x 2.4727 0.26
-dislocation 0.31*BOX 0.39*BOX screw z x 2.4727 0.26
-orient[-101][1-21][111][1-2-1] [101][-1-11]
-dislocation 0.4*BOX 0.27*BOX screw z x 2.4727 0.26
-orient[1-2-1][101][-1-11][100][010][001] -alignx 500_15yes.lmp
```

C | Appendix - Risk assessment

The mandatory risk assessment performed before the beginning of the project.

Kartlegging av risikofylt aktivitet

Dato: 03.02.2015

Enhet:

Linjeleder:

Deltakere ved kartleggingen (m/ funksjon): *Marit Olaisen (masterstudent), Christian Thaulow (veileder)*

Kort beskrivelse av hovedaktivitet/hovedprosess: Prosjektoppgave, student Marit Olaisen. ATOMISTIC MODELING OF DISLOCATIONS IN NANOPILLARS

Er oppgaven rent teoretisk? (JA/NEI): **Nei**

Signaturer: Ansvarlig veileder: *[signature] Chr. Thaulow* Student: *[signature] Marit Olaisen*

ID nr.	Aktivitet/prosess	Ansvarlig	Eksisterende dokumentasjon	Eksisterende sikringstiltak	Lov, forskrift o.l.	Kommentar
	Use of the supercomputer Vilje	Marit Olaisen	User guide	Need authorization to get access	User guide	Got authorization through a course last year
	Use of Focused Ion Beam (FIB)	Marit Olaisen	User safety manual Trainig course	FIB-course (NanoLab) Cleanroom course	User guide	
	Use of Scanning Electron Microscope (SEM) combined with indenter	Marit Olaisen/ Anette B. Hagen	User safety manual Training course	SEM training	User guide	

Risikovurdering

Dato: 18.09.2014

Enhet:

Linjeleder:

Deltakere ved kartleggingen (m/ funksjon): *Marit Olaisen (masterstudent), Christian Thaulow (veileder)*

Risikovurderingen gjelder hovedaktivitet: Prosjektoppgave, student Marit Olaisen. ATOMISTIC MODELLING OF DEFORMATION AND FRACTURE – ARCTIC MATERIALS

Signaturer: *Ansvarlig veileder:* [signature] *Student:* [signature]

ID nr	Aktivitet fra kartleggings-skjemaet	Mulig uønsket hendelse/belastning	Vurdering av sannsyn-lighet (1-5)	Vurdering av konsekvens: Menneske (A-E)	Ytre miljø (A-E)	Øk/materiell dømme (A-E)	Om-dømme (A-E)	Risiko-Verdi (menn-eske)	Kommentarer/status Forslag til tiltak
	Supercomputer Vilje	Computer system crash. Downtime.	3	A	A	C	A	A3	Need authorization to get access.
	FIB	Damage to the FIB. Downtime while waiting for engineer.	3	A	A	C	A	A3	Need Cleanroom course and FIB course to get access.
	SEM	Damage to the SEM or indenter	3	A	A	C	A	A3	SEM training. Need course to get access.
	FIB	Radiation, voltage	1	E	D	D	A	E1	Good protection
	SEM	Radiation, voltage	1	E	D	D	A	E1	Good protection

NTNU		Risikomatrise	utarbeidet av	Nummer	Dato
			HMS-avd.	HMSRV2604	08.03.2010
			godkjent av	Erstatter	
HMS/KS			Rektor		09.02.2010

Sannsynlighet vurderes etter følgende kriterier:

Svært liten	Liten	Middels	Stor	Svært stor
1	2	3	4	5
1 gang pr 50 år eller sjeldnere	1 gang pr 10 år eller sjeldnere	1 gang pr år eller sjeldnere	1 gang pr måned eller sjeldnere	Skjer ukentlig

Konsekvens vurderes etter følgende kriterier:

Gradering	Menneske	Ytre miljø Vann, jord og luft	Øk/materiell	Omdømme
E Svært Alvorlig	Død	Svært langvarig og ikke reversibel skade	Drifts- eller aktivitetsstans >1 år.	Troverdighet og respekt betydelig og varig svekket
D Alvorlig	Alvorlig personskade. Mulig uførhet.	Langvarig skade. Lang restitusjonstid	Driftsstans > ½ år Aktivitetsstans i opp til 1 år	Troverdighet og respekt betydelig svekket
C Moderat	Alvorlig personskade.	Mindre skade og lang restitusjonstid	Drifts- eller aktivitetsstans < 1 mnd	Troverdighet og respekt svekket
B Liten	Skade som krever medisinsk behandling	Mindre skade og kort restitusjonstid	Drifts- eller aktivitetsstans < 1uke	Negativ påvirkning på troverdighet og respekt
A Svært liten	Skade som krever førstehjelp	Ubetydelig skade og kort restitusjonstid	Drifts- eller aktivitetsstans < 1dag	Liten påvirkning på troverdighet og respekt

Risikoverdi = Sannsynlighet x Konsekvens
Beregn risikoverdi for Menneske. Enheten vurderer selv om de i tillegg vil beregne risikoverdi for Ytre miljø, Økonomi/materiell og Omdømme. I så fall beregnes disse hver for seg.

Til kolonnen "Kommentarer/status, forslag til forebyggende og korrigerende tiltak":
Tiltak kan påvirke både sannsynlighet og konsekvens. Prioriter tiltak som kan forhindre at hendelsen inntreffer, dvs. sannsynlighetsreduserende tiltak foran skjerpet beredskap, dvs. konsekvensreduserende tiltak.

NTNU		utarbeidet av	Nummer	Dato
		HMS-avd.	HMSRV2604	08.03.2010
		godkjent av	Erstatter	
HMS/KS		Rektor		09.02.2010

Risikomatrise

MATRISE FOR RISIKOVURDERINGER ved NTNU

KONSEKVENS						
Svært alvorlig	E1	E2	E3	E4	E5	
Alvorlig	D1	D2	D3	D4	D5	
Moderat	C1	C2	C3	C4	C5	
Liten	B1	B2	B3	B4	B5	
Svært liten	A1	A2	A3	A4	A5	
	Svært liten	Liten	Middels	Stor	Svært stor	
			SANNSYNLIGHET			

Prinsipp over akseptkriterium. Forklaring av fargene som er brukt i risikomatrisen.

Farge		Beskrivelse
Rød		Uakseptabel risiko. Tiltak skal gjennomføres for å redusere risikoen.
Gul		Vurderingsområde. Tiltak skal vurderes.
Grønn		Akseptabel risiko. Tiltak kan vurderes ut fra andre hensyn.